Tectonomagmatic characteristics of the back-arc portion of the Calama–Olacapato–El Toro Fault Zone, Central Andes

V. Acocella,[1] A. Gioncada,[2] R. Omarini,[3] U. Riller,[4] R. Mazzuoli,[2] and L. Vezzoli[5]

Received 5 December 2010; revised 1 February 2011; accepted 4 March 2011; published 2 June 2011.

[1] Post–20 Ma magmatism in the Central Andes is either localized in the magmatic arc or distributed east of it, on the Altiplano-Puna Plateau. Here there is a distinct concentration of magmatic centers on NW–SE trending lineaments, such as the Calama–Olacapato–El Toro (COT), that extends into the Eastern Cordillera to the east of the Puna. Understanding the possible genetic relationship between prominent structures and magmatic centers on these lineaments is important to elucidate the tectonomagmatic evolution of the Central Andes. We investigated the back-arc area of the COT using remote sensing, geological, structural, and petrochemical data. Our study demonstrates that this portion of the COT consists of NW–SE striking faults, formed under overall left-lateral transtension that decreases in activity toward the COT termini. Deformation on the COT occurred during and after activity of prominent N–S striking transpressive fault systems and is coeval with magmatism, which is focused on the central COT. The most evolved magmatic rocks, with an upper crustal imprint, are exposed on the central COT, whereas more primitive, mantle-derived mafic to moderately evolved magmatic rocks, are found toward the COT termini. This points to a genetic relationship between upper crustal deformation and magmatic activity that led to enhanced magma storage in the central COT. COT magmas may result either from slab steepening or episodic delamination of the asthenospheric mantle.

Citation: Acocella, V., A. Gioncada, R. Omarini, U. Riller, R. Mazzuoli, and L. Vezzoli (2011), Tectonomagmatic characteristics of the back-arc portion of the Calama–Olacapato–El Toro Fault Zone, Central Andes, *Tectonics*, *30*, TC3005, doi:10.1029/2010TC002854.

1. Introduction

[2] The study of the influence of tectonic structures on the transport, emplacement and eruption of arc magmas is important to understand tectonomagmatic processes in convergent tectonic settings. However, our knowledge of structures in magmatic arcs is frequently incomplete, as these are often obscured by volcanic rocks, and inadequate, because of the structural variability of magmatic arcs. Depending on the tectonic boundary conditions, magmatic arcs may be characterized by compressional, extensional or strike-slip structures, which have variable influence on magmatic activity [*Cole*, 1990; *Corti et al.*, 2005; *Galland et al.*, 2007]. In addition, the relationships between arc magmatism and the tectonic setting of the converging plates, in terms of erupted volumes and deformation rates, do not always follow expected trends [*Schurr et al.*, 2003; *Acocella and Funiciello*, 2010]. Thus, understanding how the structural style of an arc controls ascent, emplacement and composition of magma is a challenging task [*White et al.*, 2006] and requires an integrated scientific approach.

[3] Most of the current information on the tectonomagmatic relationships in arcs is derived from specific locations, such as New Zealand [*Wilson*, 1996; *Spinks et al.*, 2005], NE Japan [*Sato*, 1994; *Acocella et al.*, 2008], Mexico [*Tibaldi*, 1992; *Alaniz-Alvarez et al.*, 1998] and the Central Andes [*Riller et al.*, 2001; *De Silva et al.*, 2006]. In particular, back-arc magmatism in the Central Andes is largely focused in five regularly spaced NW–SE trending transverse magmatic belts [*Salfity*, 1985; *Viramonte and Petrinovic*, 1990; *Trumbull et al.*, 2006, and references therein]. These belts have been largely recognized from the alignment of magmatic centers and the presence of lineaments identified from remote sensing analyses [*Allmendinger et al.*, 1983; *Chernicoff et al.*, 2002; *Matteini et al.*, 2002]. Tectonic models suggest a predominant left-lateral motion on the faults [*Allmendinger et al.*, 1983] that can be explained by an along-strike gradient in transverse shortening in the

[1]Dipartimento Scienze Geologiche, Università Roma Tre, Rome, Italy.
[2]Dipartimento di Scienze della Terra, Università di Pisa, Pisa, Italy.
[3]Facultad de Ciencias Naturales, Universidad Nacional de Salta, CONICET, Salta, Argentina.
[4]School of Geography and Earth Sciences, McMaster University, Hamilton, Ontario, Canada.
[5]Dipartimento Scienze Chimiche e Ambientali, Università dell'Insubria, Como, Italy.

0278-7407/11/2010TC002854

Central Andes [*Riller et al.*, 2001]. However, only few structural studies have addressed the tectonomagmatic relationship [e.g., *Riller et al.*, 2001; *Richards and Villeneuve*, 2002; *Ramelow et al.*, 2006; *Petrinovic et al.*, 2006] and seismicity [*Schurr et al.*, 1999] of transverse volcanic belts in detail to date. Therefore, it is uncertain whether mapped lineaments correspond to fault zones and to what extent structural discontinuities assist transport and eruption of magmas in these zones. Thus, examination of structural and magmatic characteristics of transverse volcanic zones is expected to provide information on the cause for the presence of volcanic rocks as far as hundreds of kilometers east of the magmatic arc.

[4] This study provides a detailed structural analysis of the back-arc portion of the most prominent transverse volcanic belt of Central Andes, which corresponds spatially to the Calama–Olacapato–El Toro (COT) Fault Zone (referred to as back-arc COT, onward; Figure 1). Specifically, we explore the relationships between tectonic and magmatic activity in this zone. Notably, deformation on the COT is assessed with regard to its possible influence on the distribution of magmatic centers, as well as the generation, transport and storage of respective magmas. In this context, we also discuss tectonic scenarios involving crust and mantle dynamics in the back-arc COT.

2. Tectonic and Geological Setting of the COT

[5] The Central Andes are dominated by the ~4000 m high Altiplano-Puna Plateau, which is bounded by the Miocene to Recent magmatic arc to the west, and the Eastern Cordillera and Subandean foreland fold-and-thrust belt to the east (Figure 1). The plateau formed chiefly by E–W crustal shortening [e.g., *Isacks*, 1988; *Allmendinger et al.*, 1997; *Kley and Monaldi*, 1998; *Elger et al.*, 2005], which led to the development of internally drained, contractional sedimentary basins [*Kraemer et al.*, 1999; *Riller and Oncken*, 2003; *Sobel et al.*, 2003]. Shortening and associated basin formation in the plateau area commenced during the Eocene-Oligocene [*Jordan and Alonso*, 1987; *Allmendinger et al.*, 1997; *Kraemer et al.*, 1999; *Oncken et al.*, 2006] and continued in Quaternary times in the Eastern Cordillera and Subandean foreland [*Marrett et al.*, 1994; *Marrett and Strecker*, 2000]. In the Puna, compressive deformation is distributed, whereas localized basement-involved folding and thrusting is more typical for the Eastern Cordillera [*Kley*, 1996].

[6] Kinematic regimes in the Puna and Eastern Cordillera are characterized by NW–SE and NE–SW shortening directions, inferred from small-scale faults [*Marrett et al.*, 1994]. These shortening directions were attributed to deformation increments operating during the Miocene and Pliocene and during the Pliocene to Recent times, respectively [*Marrett et al.*, 1994; *Cladouhos et al.*, 1994]. The change in the shortening directions has been related to the change in the direction and rate of absolute motion of the South American Plate [*Marrett and Strecker*, 2000]. Alternatively, the variation in the shortening directions can be explained by the variation in the orientation and kinematics of prominent fault zones, and, as a consequence, of orogen-parallel extension [*Riller and Oncken*, 2003; *Maffione et al.*, 2009]. Neogene deformation in the plateau area is characterized by orogen-parallel extension and overall southward and eastward propagation [*Riller and Oncken*, 2003; *Deeken et al.*, 2006]. This is possibly induced by middle to lower crustal orogen-parallel channel flow in the southern Central Andes [*Hindle et al.*, 2005; *Ouimet and Cook*, 2010].

[7] NW–SE striking lineaments, such as the COT, appear as first-order fault zones of the Altiplano-Puna Plateau (Figure 1) [*Salfity*, 1985]. These fault zones are associated with Neogene magmatic centers, collectively known as transverse magmatic belts [*Viramonte et al.*, 1984; *Viramonte and Petrinovic*, 1990; *Matteini et al.*, 2002]. Their basement, in the Puna and Eastern Cordillera, consists mainly of low-grade metamorphic rocks of the Late Neoproterozoic to Early Cambrian Puncoviscana Formation [*Turner*, 1964], and Ordovician metamorphic rock and syntectonic granites [*Hongn and Riller*, 2007; *Ramos*, 2008, and references therein]. These rocks are unconformably overlain by Cretaceous and Tertiary sedimentary rocks of the Salta Group, which formed during a phase of continental rifting prior to Andean orogenesis [*Salfity and Marquillas*, 1994].

[8] The back-arc COT consists of approximately 21 major and highly different magmatic centers, including explosive vents, calderas, composite stratovolcanoes, monogenetic cones, lava domes and plutons that have been active since Miocene times (Figure 2). In the back-arc portion of the COT, next to the Miocene-Quaternary volcanic arc, volcanic activity consists of the geometrically aligned, closely spaced andesitic-dacitic stratovolcanoes of Rincon, Tul-Tul, Del Medio and Pocitos [*Koukharsky and Munizaga*, 1990; *Matteini*, 2001; *Matteini et al.*, 2002]. In its central sector, COT includes the Quevar and Aguas Calientes calderas, that erupted voluminous silicic ignimbrites and tephra, individual phreatoplinian vents, such as Tocomar and Ramadas, and Quaternary mafic effusive centers, i.e., Tuzgle, Negro de Chorrillos and San Jerónimo [*Schreiber and Schwab*, 1991; *Deruelle*, 1991; *Coira and Kay*, 1993; *Goddard et al.*, 1999; *Petrinovic*, 1999; *Petrinovic et al.*, 2005, 2006, 2010]. To the east, close to the Eastern Cordillera, COT includes the partially dissected andesitic-dacitic Chimpa stratovolcano [*Arnosio*, 2002] and the Negra Muerta volcanic complex. The latter includes a caldera-forming event, followed by lava flows, rhyodacitic dykes and domes [*Petrinovic et al.*, 1999, 2005; *Ramelow et al.*, 2006]. In this sector, dacitic domes, notably El Morro, Organullo and Rupasca, have also been recognized [*Viramonte et al.*, 1984; *Blasco et al.*, 1996; *Petrinovic et al.*, 1999; *Arnosio et al.*, 2005]. The easternmost magmatic centers of the COT are found in the Eastern Cordillera and include middle Miocene intrusions, such as Las Burras and Acay, that were eroded during exhumation of the Cordillera, andesitic-dacitic lava domes and flows of the Almagro and young mafic effusive centers of the Los Gemelos and El Saladillo centers [*Krallmann*, 1994; *Hongn et al.*, 2002; *Matteini et al.*, 2002; *Haschke et al.*, 2005; *Gioncada et al.*, 2006; *Guzmán et al.*, 2006; *Mazzuoli et al.*, 2008; *Vezzoli et al.*, 2009].

[9] During the Neogene, the COT accomplished approximately 20 km of left-lateral displacement [*Allmendinger et al.*, 1983]. In addition to the lateral displacement, the COT is also locally characterized by a component of N–S extension [*Riller et al.*, 2001; *Petrinovic and Colombo Piñol*, 2006]. Overall left-lateral transtension may have facilitated the ascent of magma [*Mazzuoli et al.*, 2008] and

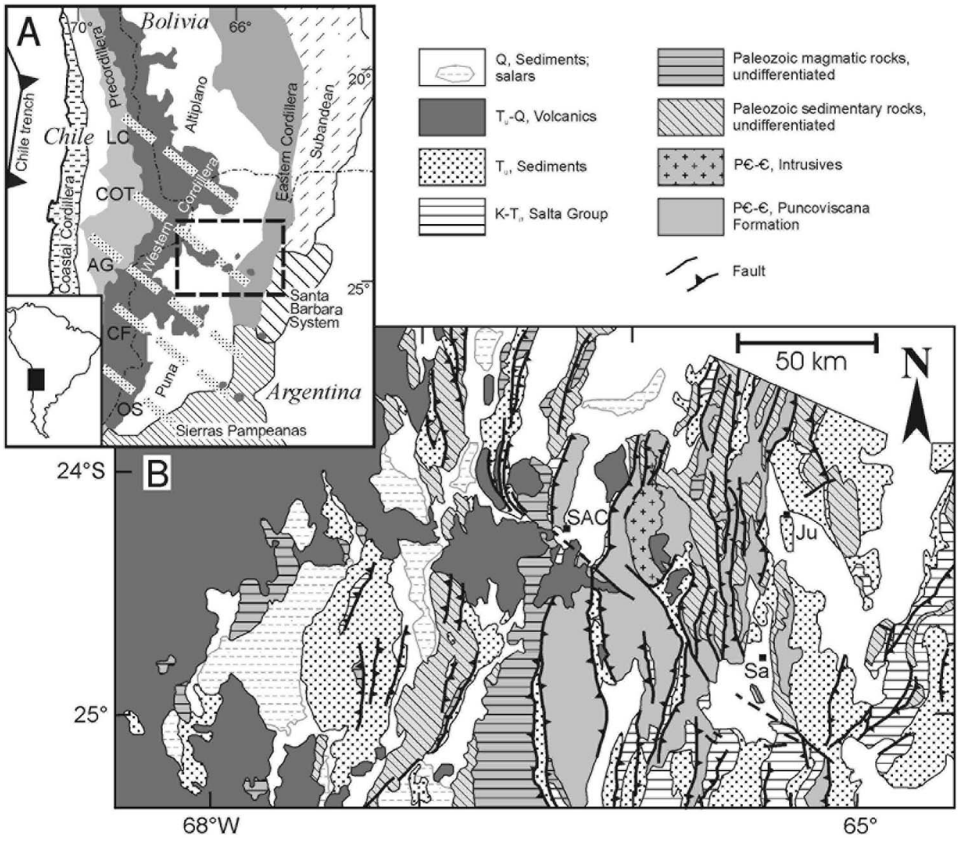

Figure 1. (a) Structure of the Central Andes, highlighting the back-arc area, characterized by several ~NW–SE trending lineaments associated with magmatic activity (dashed lines). These include the Lipez-Coranzuli (LC), Calama–Olacapato–El Toro (COT), Archibarca-Galan (AG), Culumpaja–Farallon Negro (CF), and Ojos del Salado (OS). (b) Simplified geological map, and related main structural units and regional faults, of the back-arc part of the COT, from the current volcanic arc to the Eastern Cordillera (location shown by dashed rectangle in Figure 1a). SAC, San Antonio de los Cobres; Sa, Salta; Ju, Jujuy.

caldera formation [*Riller et al.*, 2001; *Caffe et al.*, 2002; *Chernicoff et al.*, 2002; *Matteini et al.*, 2002; *Ramelow et al.*, 2006; *Petrinovic et al.*, 2005, 2006], but this kinematic regime remains to be ascertained for the COT.

3. Results

3.1. Remote Sensing Analysis

[10] Acquisition of original remote sensing data and a compilation of known fault zones allows us to define the first-order, largest structural elements of the back-arc part of the COT, from the volcanic arc to the Eastern Cordillera (Figure 2). Remote sensing data are obtained from satellite images (available at http://earth.google.com/intl/it, with a mean resolution of a few tens of meters) and digital elevation models (DEM) (available at http://www.geomapapp.org, with a resolution of 90 m). Satellite images and DEMs were used to identify, map and characterize fault zones, in terms of strike and length.

[11] Lineaments in the back-arc COT trend N–S, i.e., parallel to the regional structural grain of the area, and NW–SE (Figure 2). Lengths of individual NW–SE trending lineaments are up to several tens of kilometers and are most prominent in the central part of the study area, i.e., west of San Antonio de los Cobres (Figure 2). These NW–SE trending lineaments progressively decrease in spatial density and length toward the northeast and southwest. In the western COT, the lineaments are rare, and here the presence of NW–SE trending systems may be evident by the alignment of the Tul-Tul, Del Medio and Pocitos volcanoes (Figure 2). In many cases, as to the south of the San Antonio de los Cobres area, the NW–SE trending lineaments crosscut the N–S trending ones; in other cases, as in the central part of the area, N–S trending lineaments merge with NW–SE trending ones, forming sigmoidal lineament patterns (Figure 2).

[12] A compilation of fault zones from published geological maps [*Hongn and Seggiaro*, 2001; *Marrett et al.*, 1994; *Blasco et al.*, 1996] shows the pervasive presence of N–S trending regional fault systems, with either reverse or normal sense of displacement (Figure 2). However, NW–SE trending faults have also been identified, largely in the central part of the studied area, where their length and spatial density is maximal, and generally coincide spatially with the NW–SE trending lineaments. The kinematics of NW–SE striking faults is not well known, but sometimes reported as left-lateral transtensive [*Marrett et al.*, 1994, and references therein]. Their activity dates broadly to the

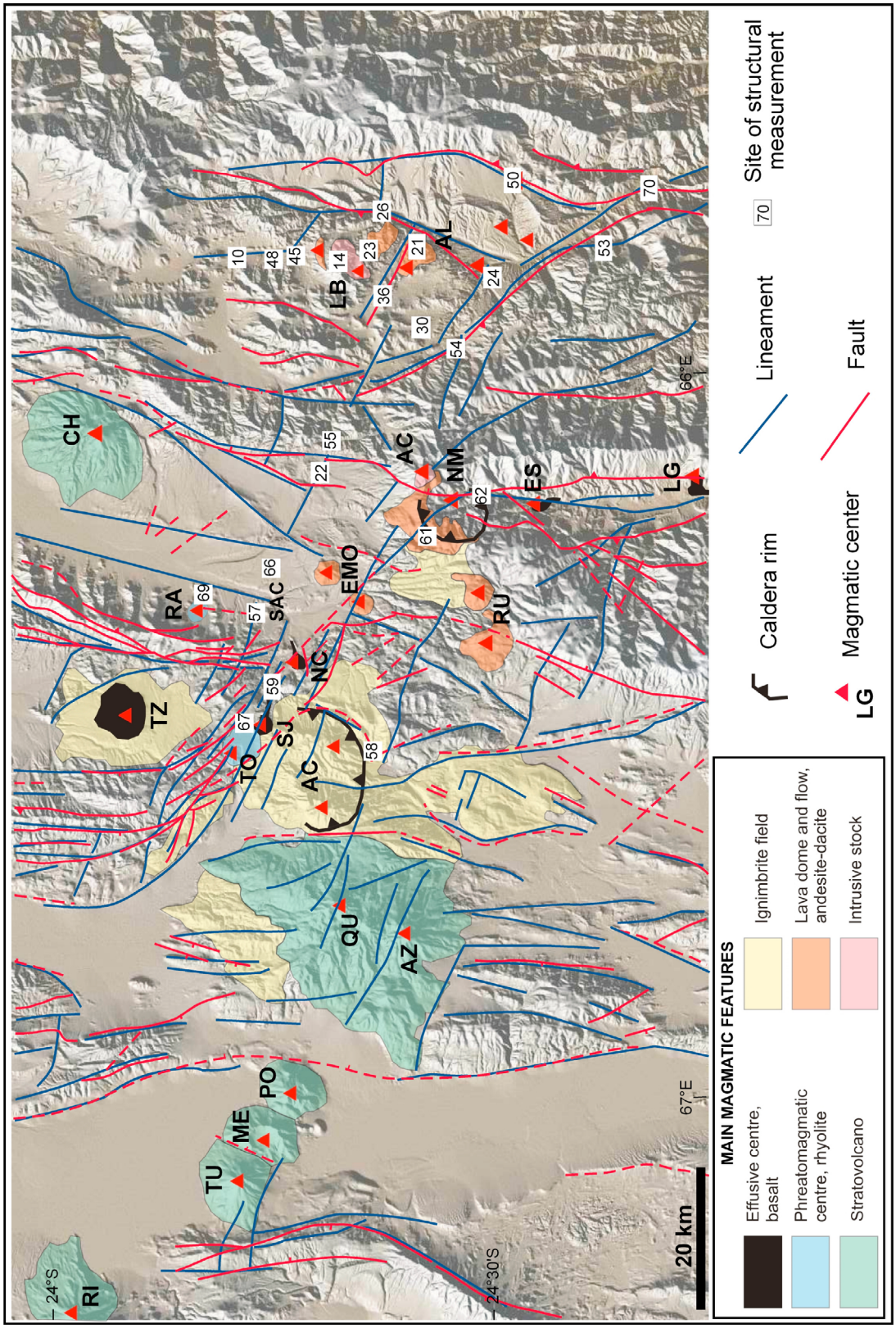

Figure 2. DEM of the back-arc COT, reporting the extent and the main features of the magmatic deposits associated with the activity of 21 major centers (red triangles). RI, Rincon; TU, Tul-Tul; ME, El Medio; PO, Pocitos; QU, Quevar; AZ, Azufrero; TO, Tocomar; TZ, Tuzgle; SJ, San Jeronimo; NC, Negro de Chorillos; AC, Aguas Calientes; EMO, El Morro–Organullo; NM, Negra Muerta; AC, Acay; RA, Ramadas; CH, Chimpa; RU, Rupasca; ES, El Saladillo; LG, Los Gemelos; LB, Las Burras; AL, Almagro-El Toro. The major lineaments (in blue), also visible from satellite maps, and the major faults (in red, as shown on available maps) are also reported. Numbers refer to the location of the sites of structural analysis. See text for further details.

Table 1. Analysis of the Fault Slip Data[a]

		P-T Method			Direct Inversion Method					Numeric Dynamic Analysis							
Site	N	P	B	T	$\sigma1$	$\sigma2$	$\sigma3$	R(stress)	NEV	$\lambda1$	$\lambda2$	$\lambda3$	R(strain)	NEV	Method	Max. Age	Geologic Unit[b]
10	10	036/12	149/68	301/20	185/04	276/12	079/77	0.55	1	036/17	158/17	299/23	0.43	0	NDA	<Paleozoic	Puncoviscana Formation
14	9	073/45	289/42	189/09	293/84	033/01	123/06	0.62	2	078/57	285/30	188/13	0.67	1	NDA	<14 Ma	Las Burras granite (a)
21	31	260/66	147/09	031/01	259/84	050/05	140/03	0.38	9	124/74	296/16	026/02	0.86	8	NDA	<Paleozoic	Puncoviscana Formation
22	21	157/83	357/52	255/11	268/11	358/03	102/78	0.23	9	068/78	171/03	261/11	0.88	11	Invers.	<Paleozoic	Puncoviscana Formation
23	25	278/19	104/75	191/02	279/26	091/64	187/03	0.49	10	275/23	098/67	006/01	0.73	8	NDA	<14 Ma	Las Burras granite (a)
24	5	180/84	349/09	079/00	172/39	295/34	050/33	0.45	0	174/84	348/06	078/01	0.53	0	NDA	<11 Ma	Las Cuevas volcanic member (a)
26	17	237/47	046/58	161/13	356/88	196/02	106/01	0.37	4	298/84	060/03	151/05	0.47	2	NDA	<Paleozoic	Puncoviscana Formation
30	15	224/23	059/61	313/04	172/53	002/37	269/05	0.85	5	214/12	041/77	305/02	0.75	4	NDA	<Paleozoic	Puncoviscana Formation
36	12	094/66	301/31	020/03	108/69	261/19	354/09	0.23	1	274/71	107/19	016/04	0.66	0	NDA	<7.4–7 Ma	Lavas, Almagro B member (a)
45	17	069/04	139/75	336/05	274/10	009/24	162/64	0.19	7	065/11	257/79	155/02	0.56	2	NDA	<14 Ma	Las Burras granite (a)
48	14	229/15	301/77	329/01	194/49	022/40	289/04	0.90	6	228/56	047/34	137/01	0.66	1	NDA	<Paleozoic	Puncoviscana Formation
50	2	136/20	041/16	282/59											P-T	<Cretaceous	Sedim. Yacoraite Formation (Salta Group)
53	6	335/44	213/19	111/31	017/10	109/09	239/77	0.55	0	355/32	240/35	115/39	0.83	1	NDA	<Cretaceous	Sedim. Yacoraite Formation (Salta Group)
54	5	256/01	344/08	320/87	121/13	028/15	249/70	0.70	1	120/20	218/19	349/62	0.79	1	Invers.	<Paleozoic	Puncoviscana Formation
55	3	123/31	281/57	027/10											P-T	<Paleozoic	Puncoviscana Formation
59	5	355/77	207/10	117/06	069/66	209/19	304/14	0.28	0	359/76	210/12	118/07	0.46	0	NDA	<10 Ma	Taiamar ignimbrite (b)
61	24	006/65	193/31	103/07	270/82	018/02	109/07	0.22	4	343/74	194/14	102/08	0.31	5	Invers.	<7.3 Ma	Negra Muerta andesite lava (c)
62	12	275/65	172/13	077/12	007/27	246/45	116/33	0.46	4	302/79	191/04	100/10	0.27	2	NDA	<Paleozoic	Puncoviscana Formation
66	5	314/72	056/09	150/14	310/22	214/15	092/63	0.89	2	326/74	061/02	152/16	0.41	0	NDA	<2 Ma	Continental alluvial deposits
67	25	068/23	200/59	325/14	140/80	295/09	026/04	0.20	8	070/42	240/48	335/05	0.82	6	NDA	<1.5–0.5 Ma	Tocomar pyroclastic units (d, e)
69	3	318/15	070/51	213/35											P-T	<8.5 Ma	Ramadas Pyroclastic Units (f)
70	13	003/05	151/47	267/26	162/42	001/46	261/10	0.38	5	006/07	105/54	271/35	0.88	2	NDA	<Cretaceous	Sedimentary continental

[a]The table lists the orientation (strike and dip) of the stress and strain axes, as obtained using the P-T, direct inversion, and numeric dynamic analysis methods for the measurement sites with ≥ 4 faults (see text for details). Visualization of the axes is reported in Figure 7. The table also shows the age, lithology, and geologic units (with associated reference) of the rocks hosting the deformation. Blank cells represent insufficient data.

[b]References are as follows: a, *Mazzuoli et al.* [2008]; b, *Petrinovic et al.* [2010]; c, *Ramelow et al.* [2006]; d, *Aquater* [1980]; e, *Petrinovic et al.* [1999]; f, *Viramonte et al.* [1984].

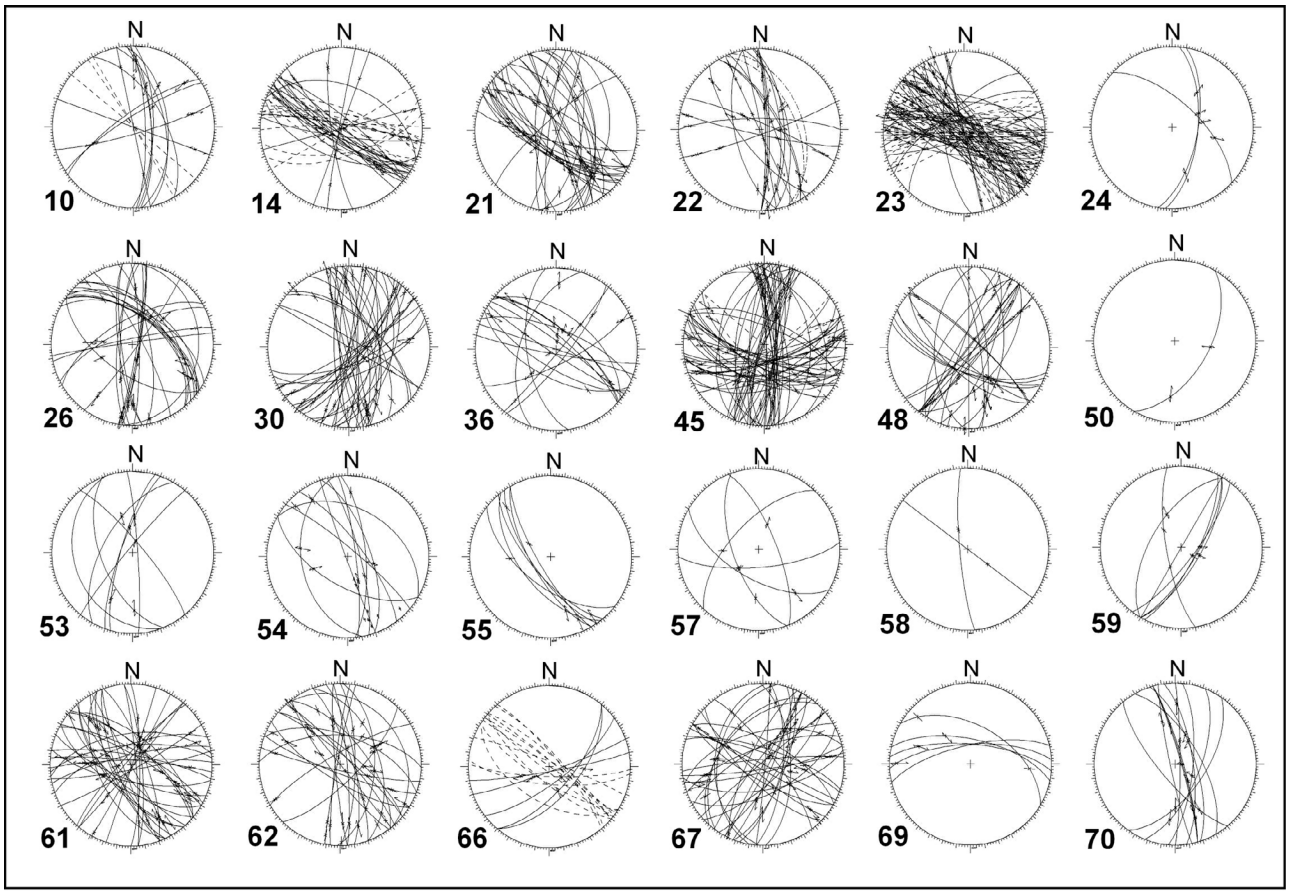

Figure 3. Collected structural field data set relative to the back-arc COT. The data are plotted on lower hemisphere equal-area projections according to respective sites (numbered; for location see Figure 2); solid lines, faults; dashed lines, joints; arrows within the plots represent sense of movement, as inferred from striations.

Neogene, as they mostly affect sedimentary deposits of this age [*Blasco et al.*, 1996].

[13] The spatial congruence, in location and orientation, of lineaments inferred from remote sensing with faults evident from geological maps suggests that a significant portion of the lineaments formed by faulting. Moreover, many magmatic centers are aligned in correspondence with NW–SE and N–S trending lineaments and faults. The congruence of remotely sensed and mapped faults also shows that the NW–SE systems are more abundant and prominent, in terms of spatial density and length, in the central COT area (Figure 2). Here, the COT reaches its maximum width of approximately 50 km, and narrows toward its eastern and western termini (reaching a width of ~20 km and < 10 km, respectively).

3.2. Structural Analysis

[14] Structural field data were collected mainly on the major NW–SE and N–S trending fault systems of the back-arc COT, in order to better characterize their geometry, kinematics, principal paleostress directions and relative age. The data include faults and, subordinately, extension fractures (Figure 3). Identification and measurement of slickenlines on fault surfaces allowed us to constrain the fault kinematics. The slickenlines consist of striations, sometimes associated with mineral fibers. The sense of slip on the faults was also determined by the orientation of microscale and mesoscale indicators, such as stylolites, extension fractures, Riedel shears, steps and chatter marks. Our structural analysis includes also data by *Acocella et al.* [2007] and *Mazzuoli et al.* [2008].

[15] Deformed lithologies include metasedimentary, sedimentary (marine and continental), intrusive and volcanic (lavas and pyroclastites) deposits (Table 1). The age of the rocks affected by brittle deformation ranges from the Precambrian metasedimentary Puncoviscana Formation to Quaternary alluvial deposits (Table 1) and allows us to estimate the maximum age of brittle deformation for various locations (Figure 2). Hence, maximum deformation ages vary from Paleozoic to Quaternary, but minimum ages could not be determined.

[16] In general, extension fractures and faults of the back-arc COT strike mostly NW–SE and N–S and dip to the east (Figures 3 and 4a). However, the separation of extension fractures and faults shows that the former exclusively have a NW–SE to E–W trend (Figures 4c and 4d). The extension fractures and faults usually have a high angle to subvertical dip (Figure 4b). Therefore, the strike of the main structures observed in the field (Figure 4) is broadly consistent with

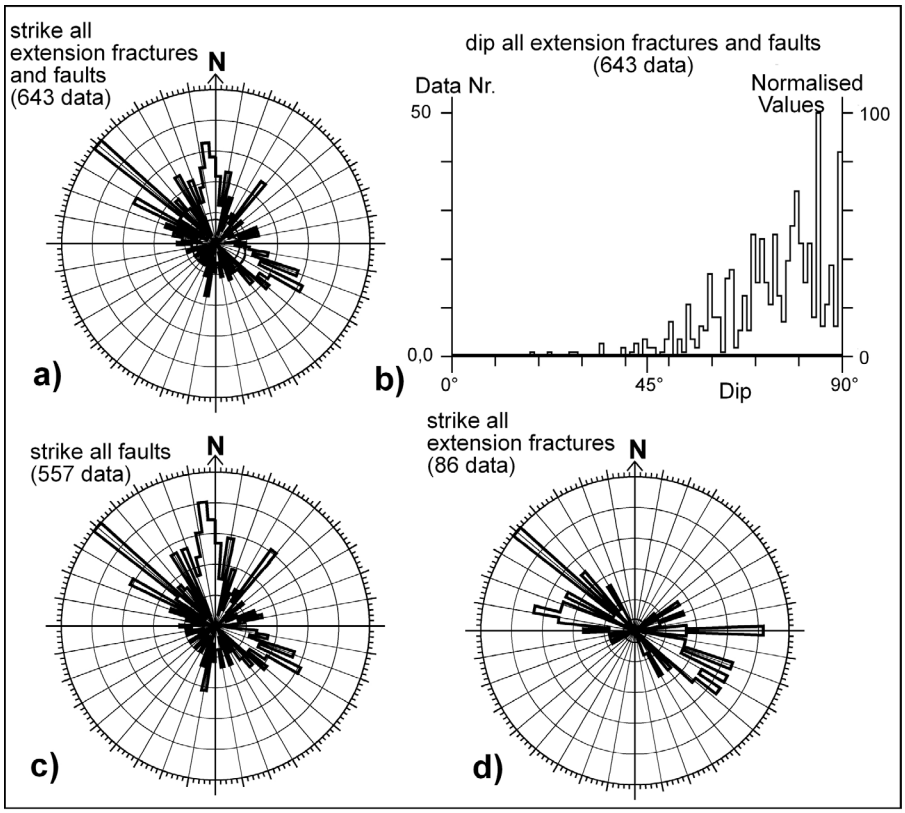

Figure 4. Geometric characteristics of all faults recorded from the back-arc COT. (a) Strike and (b) dip of extension fractures and faults. (c) Strike of faults and (d) extension fractures.

that obtained from remote sensing and published geological maps (Figure 2).

[17] Fault crosscutting relationships at 7 sites show that the N–S trending faults are older than the NW–SE trending faults, whereas the opposite has been observed at 2 sites. These relationships, as well as the above mentioned coeval development of the ~N–S and ~NW–SE trending lineaments show that (1) some COT-parallel structures postdate the activity of the ~N–S trending regional structures and (2) other COT-parallel and ~N–S regional fault systems are coeval.

[18] The geometric and kinematic features of the COT-parallel faults and extension fractures have been further investigated (Figure 5). The back-arc COT lineaments are characterized by an overall N60°W trend (Figure 2); in order not to exclude from our analysis any fault potentially related to the COT, even though with a slightly different strike, we have considered all fractures striking between N20°W and N100°W, that is N60°W ± 40°. All faults included within this wide range show a preferred strike, peaking at ~N50°W. Conversely, the extension fractures show two main clusters, coinciding with a ~N50°W strike and, subordinately, an ~E–W one (Figures 5a and 5b). The dip of faults and extension fractures varies from high angle to subvertical and is consistent with that of the entire fracture population (Figure 3). The slip of the faults is expressed through the pitch angle of the slickenlines, which ranges from 0° to 180° and corresponds to pure strike-slip motions, whereas pitches of 90° correspond to pure dip-slip motions. The pitch distribution has been reported, in Figure 5d–5f as a function of the displacement, as estimated from marker offsets. Large faults have displacements > 10 m, medium faults have displacements between 1 and 10 m, and minor faults have displacements < 1 m. Independently of the considered range of fault displacements, COT-parallel structures have a wide kinematic variability, ranging from dip slip to strike slip. However, a predominance of transtensive motions can be derived from the three displacement domains (Figures 5d–5f). More specifically, the observed dip-slip component is normal at 40 faults, whereas it is reverse at 4 faults. The strike-slip component is left lateral at 62 faults, whereas it is right lateral at 14 faults.

[19] The spacing of the COT-parallel faults varies considerably and appears to correlate with their displacement magnitudes. On the one side, major fault zones, with displacement of several tens of meters at least are associated with cataclasite, and found within less frequent but narrower (less than a few tens of meters wide) zones of deformation. An example in Figure 6a shows a NW–SE trending area characterized by pervasive cataclasite, in which relicts of COT-parallel faults are found. As the amount of cataclasite and fracturing decrease away toward the NE and SW sides, the area shown in Figure 6a represents the core of a major damage zone associated with COT-parallel faults, similar to what is observed elsewhere [*Gudmundsson et al.*, 2010]. These cataclasite zones usually have a distinct geomorphologic expression, such as the presence of fault scarps, evident at site 21 (Figures 2 and 3). On the other hand, minor fault zones, where each fault has a displacement of a very few tens of cm, consist of regularly spaced (a few meters)

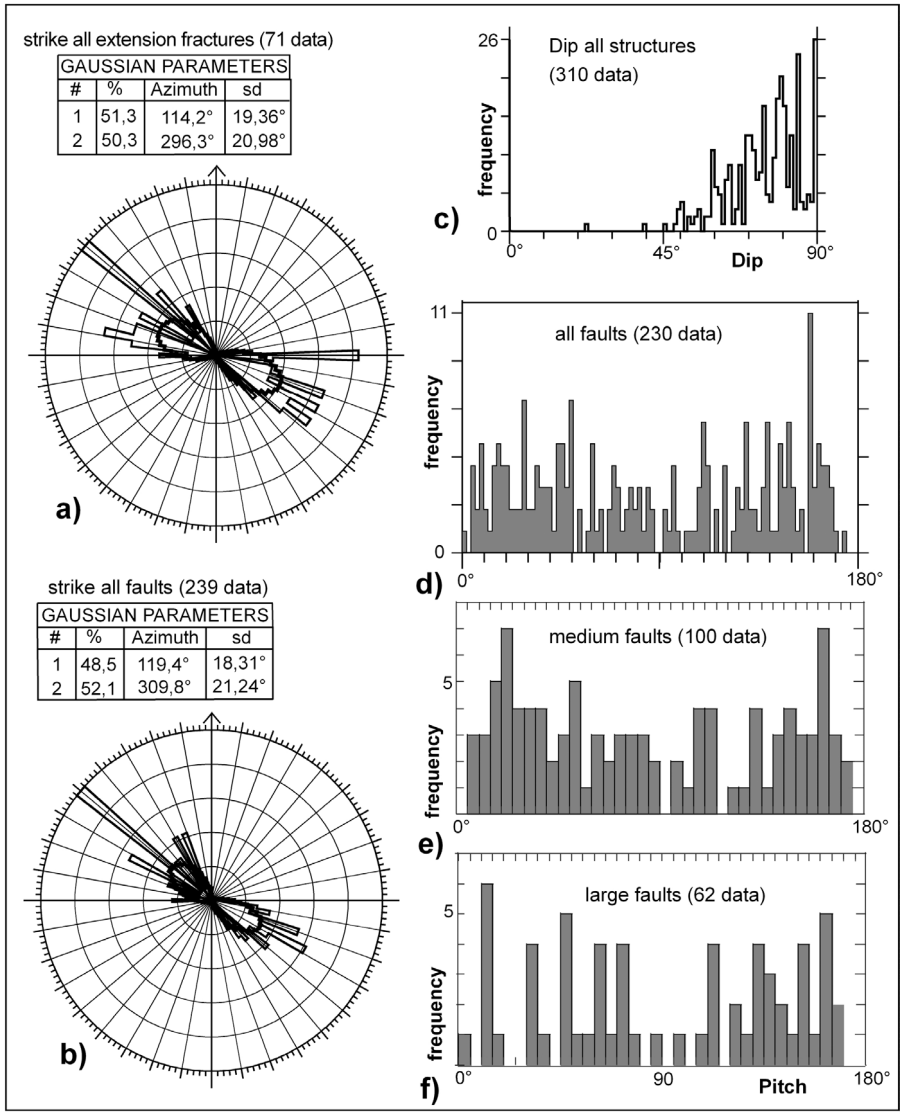

Figure 5. Geometric and kinematic features of the ~NW–SE (striking between N20°W and N100°W) extension fractures and faults. Strike of (a) extension fractures and (b) faults. (c) Dip of faults. (d–f) Distribution of fault pitch as a function of the displacement on the fault (see text for details).

fault segments, forming a tens of meters wide fault zone, without any evident geomorphic expression, as observed at site 26 (Figure 6b). The motion of these minor fault zones also points to overall transtension.

3.3. Fault Slip Analysis

[20] In order to further determine the kinematic regime, notably local shortening and extension directions, of the back-arc COT, the orientation of small-scale faults and associated sense of slip was measured at 23 sites (Table 1; see also auxiliary material).[1] The sense of slip on the faults was inferred from the orientation and geometry of stylolites, dilation fractures, Riedel shears, steps in mineral fibers and chatter marks. The fault population consists chiefly of ~NW–SE striking sinistral and normal faults, ~N–S striking dextral, dextral oblique and reverse faults, as well as ~NE–SW striking normal and oblique normal faults (Figure 7). NW–SE striking sinistral and (oblique) normal faults are more prevalent at sites from within the central COT corridor (delimited by yellow stippled lines in Figure 8). Conversely, strike-slip and reverse faults are more developed outside the central COT corridor (Figure 7).

[21] For each fault population per site, the principal strain and paleostress directions were calculated (Table 1) using the P-T method [*Turner*, 1953], the direct inversion method [*Angelier and Goguel*, 1979] and the Numeric Dynamic Analysis (NDA) [*Spang*, 1972]. These methods adhere to the Mohr-Coulomb Criterion for brittle fracturing. The P-T method and NDA result in rudimentary strain tensors, i.e., directions of the three principal reciprocal strains ($\lambda_1 > \lambda_2 > \lambda_3$) and the strain ratio ($R_{strain}$). For these methods, we assumed that the angle between λ_1 and the maximum resolved shear strain, generally believed to be parallel to the

[1] Auxiliary materials are available at ftp://ftp.agu.org/apend/tc/2010TC002854.

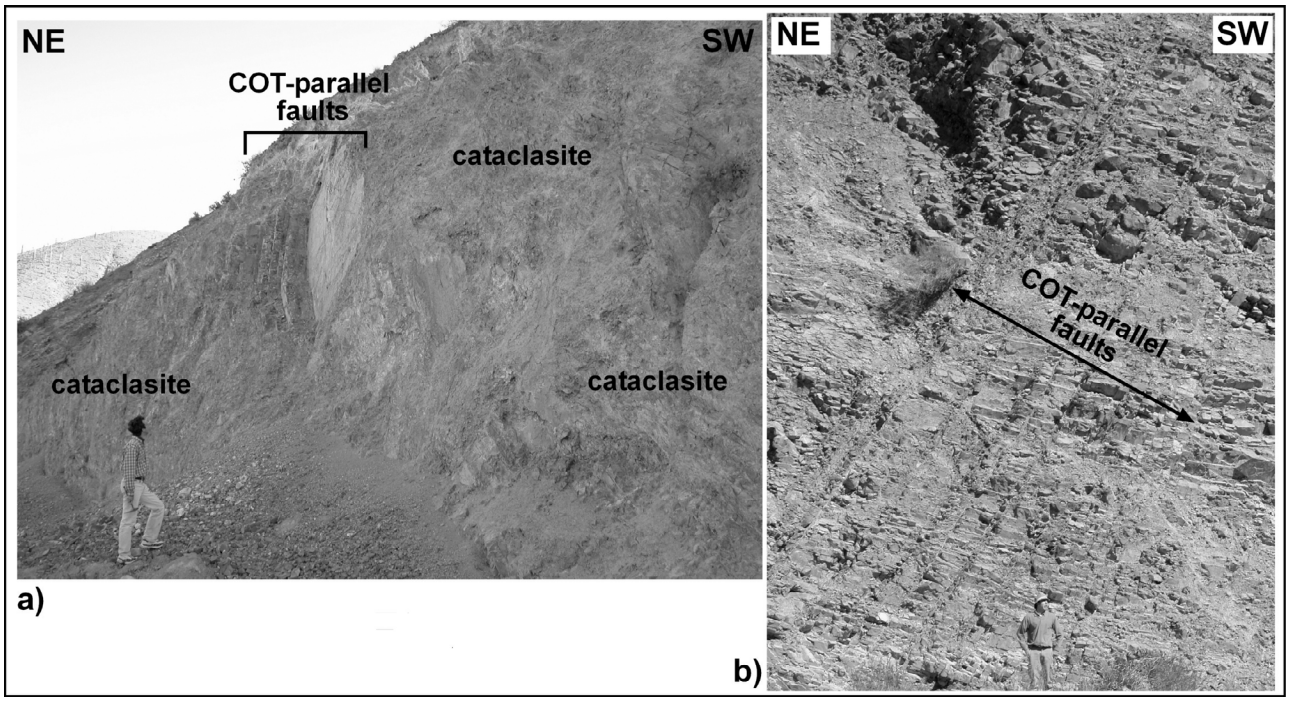

Figure 6. Field examples of (a) major and (b) minor COT-parallel fault zones, characterized by a more focused and pervasive (site 21; Figure 3) and a broader less intense area of deformation (site 26; Figure 3), respectively. In particular, Figure 6a shows a NW–SE trending area characterized by pervasive cataclasite, in which relicts of COT-parallel faults are found.

mineral lineations on the shear faults, is 30°, which is within the limits of experimentally obtained values for this angle [*Byerlee*, 1968]. The direct inversion method provides solutions in terms of rudimentary paleostress tensors, notably the directions of principal paleostress axes ($\sigma_1 > \sigma_2 > \sigma_3$) and the stress ratio ($R_{stress}$). In addition, the direct inversion method and NDA give the number of fault planes whose measured slip senses are opposite to the ones predicted by a particular solution (indicated as "negative expected value" *nev* in Table 1). For further assumptions each method relies on, see reviews by *Twiss and Unruh* [1998] and *Sperner and Zweigel* [2010].

[22] The direct inversion method and NDA require at least four independent fault orientations per site. As four sites contained less than four faults (Figure 3), 19 sites were used for brittle fault analysis to constrain the shortening and extension directions of the back-arc COT (Table 1 and Figures 7 and 8). The choice of which method was used for a given fault population was based on the *nev* (Table 1) and the best fit of principal axes orientations with respect to fault orientation and slip sense (Figure 8). We found that shortening and extension directions of most brittle fault populations from COT were best represented by the NDA, whereby the P-T method resulted in similar paleostrain solutions (Table 1). Only for three sites the direct inversion method was preferred over the NDA. We, therefore, interpret the brittle fault populations of the back-arc COT in terms of paleostrain.

[23] Principal shortening and extension axes projected to map view show a distinct spatial pattern within the back-arc COT (Figure 8). Fault populations away from the central corridor of COT are spatially associated with lower-order (smaller in dimension), ~N–S or ~NW–SE striking reverse faults or may be related to the formation of the Negra Muerta caldera (sites 61 and 62). Away from this central corridor, shortening directions are oriented crudely ~N–S and extension directions are oriented ~ESE–WNW. The average strain ratio for these fault populations is 0.56 (Table 1), suggesting plain strain conditions. Shortening directions change progressively in orientation from northerly toward ~ESE–WNW with proximity to the central COT corridor (i.e., sites 10, 48 and 45 north of the corridor, and sites 70 and 53, south of the corridor). Within the central COT corridor, shortening directions are vertical and stretching directions are oriented crudely N–S (see diagram displaying COT λ_1- and λ_3 axes in Figure 7). Here, faults are spatially associated with lower-order faults striking ~WNW–ESE, i.e., parallel to the overall strike of the COT. The average strain ratio is 0.7 (Table 1), indicating that axial extension is more prevalent within the central COT. The obliquity between calculated shortening directions and lower-order faults points to a sinistral component of displacement on these faults. Vertical shortening and sinistral displacement amount to sinistral transtension within the central COT corridor.

4. Age and Composition of COT Magmatic Rocks: An Overview of Existing Data

[24] In the last decade, several studies focused on the evolution of the Miocene and younger back-arc magmatism in the Central Andes, notably with regard to the transverse volcanic belts (e.g., see references in the works by *Trumbull*

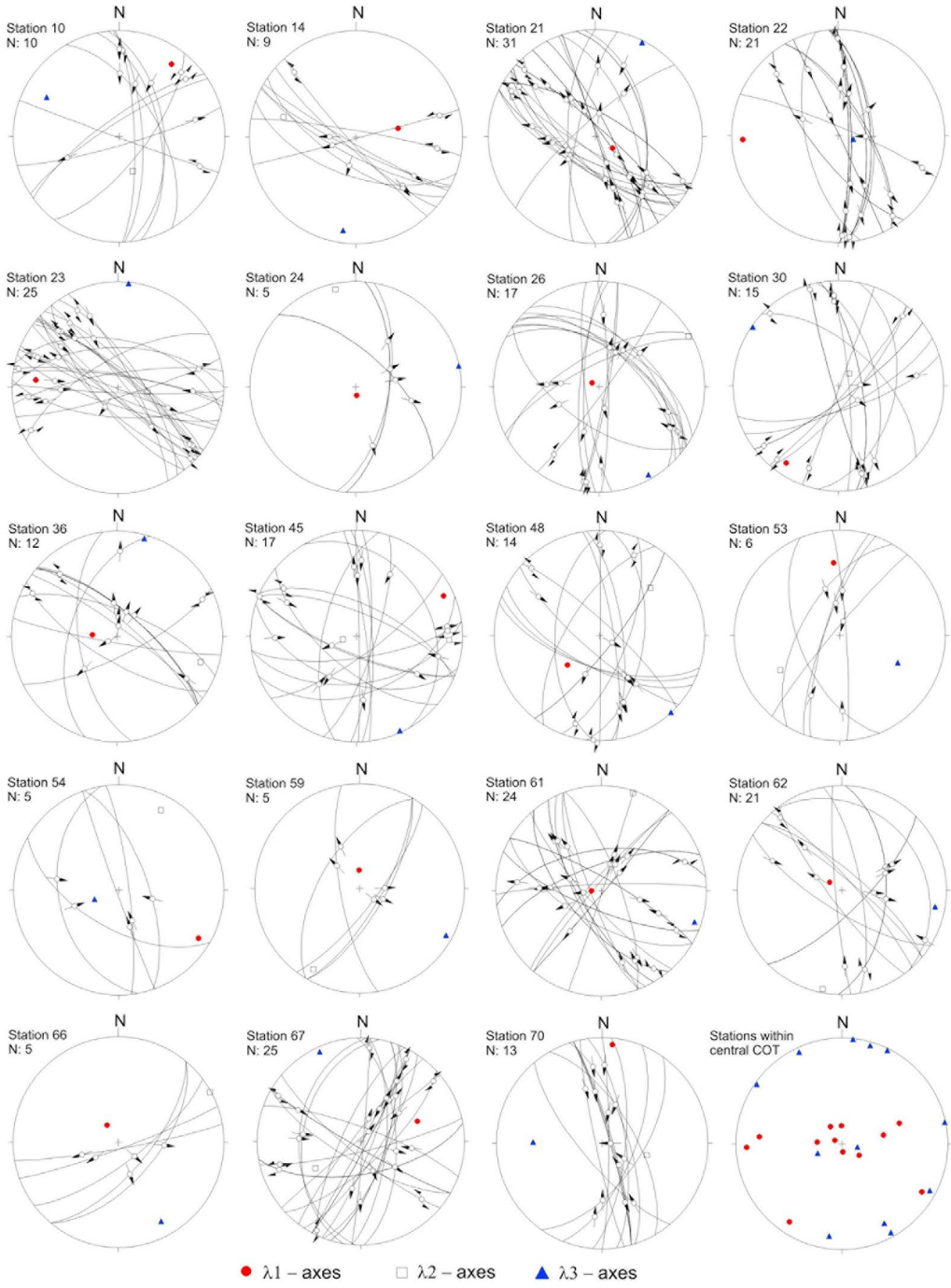

Figure 7. Structural data and related strain and stress axes for individual sites (for location of sites see Figure 2) characterized by fault slip analysis, with ≥ 4 faults per site. The data are plotted on lower hemisphere equal-area projections. Quantities of the rudimentary strain and stress tensors are listed in Table 1.

et al. [2006] and *Mazzuoli et al.* [2008]). In this section, we consider these studies to provide an overview of the main compositional and age variation for the COT magmatic rocks (Figure 9a).

[25] As a general consideration, the magmatic rocks along the back-arc COT are compositionally diverse, ranging in silica from 51 to 75 wt % (Figure 9b and Table 2) and include mafic rocks with different affinity (basaltic andesites and shoshonites; Table 2). Most volcanic deposits on the COT are andesites and dacites. Approximately 650 km^3 of mainly dacitic magma are estimated to have been erupted from the Aguas Calientes center alone [*Petrinovic et al.*, 2010]. Rhyolites are represented by some phreatomagmatic tuffs and lavas in the central sector of the back-arc

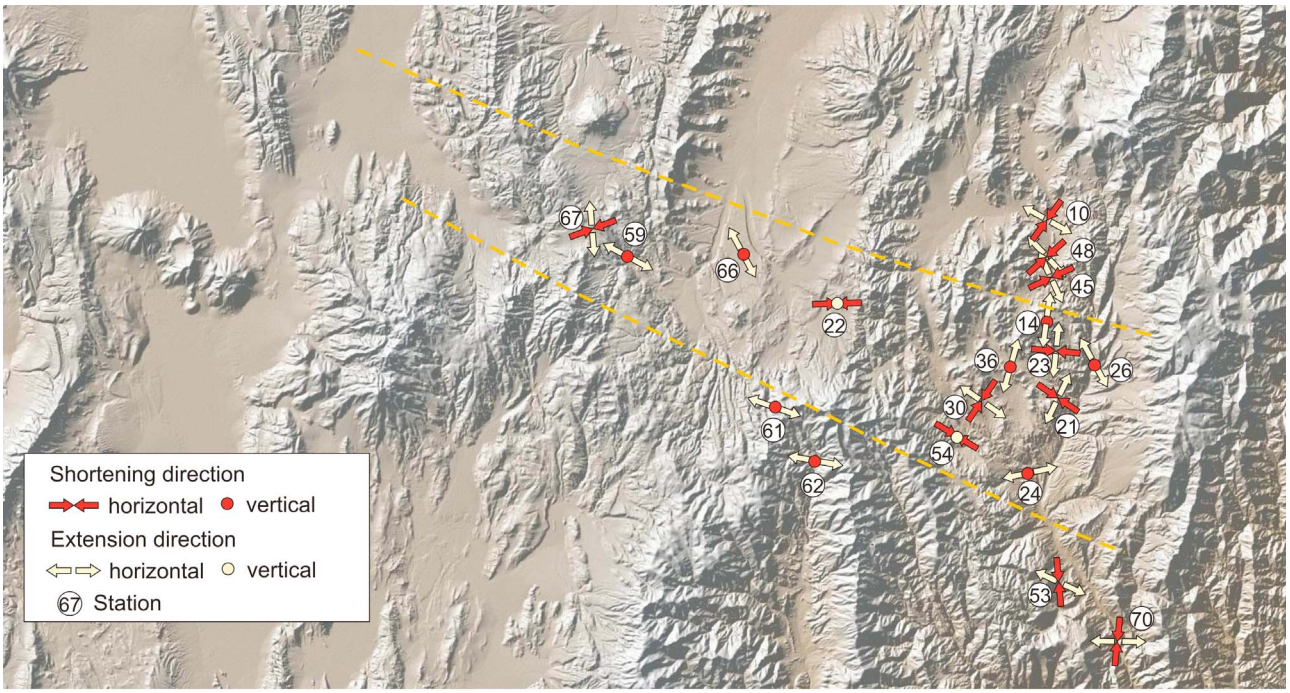

Figure 8. Map view of the distribution of the orientation of the P and T axes derived from the structural analysis along the back-arc COT. The corridor corresponding to the central portion of the COT is delineated by dashed lines.

belt (Ramadas and Tocomar [*Viramonte et al.*, 1984; *Petrinovic and Colombo Piñol*, 2006]). Mafic rocks are represented by basaltic andesites in the western sector (Tul-Tul [*Matteini et al.*, 2002]) and eastern sector (Chimpa [*Arnosio*, 2010]; Almagro [*Mazzuoli et al.*, 2008]) and by shoshonites of 0.7–0.03 Ma monogenetic centers in the central and eastern sector of the back-arc (San Jeronimo, Negro de Chorrillos, Los Gemelos and El Saladillo [*Deruelle*, 1991; *Schreiber and Schwab*, 1991; *Guzmán et al.*, 2006]).

[26] Available age data (see references in Table 2) show that magmatic activity on the back-arc COT occurred almost uninterruptedly between 17.15 and 5.3 Ma, starting in the central and eastern sectors, and affecting the entire back-arc COT between ~12 and 5.3 Ma, with a peak at 12–8 Ma (Figure 9c). A gap in the volcanic activity between 5.3 and 1.5 Ma (Tocomar [*Aquater*, 1980]) was followed by volcanism in the central Puna and Eastern Cordillera (Figure 9c). Mafic magmas were erupted at 12, 7–5 and < 1.5 Ma (Figure 9d).

[27] There is no apparent trend in age or composition for the magmatic products transverse to the strike of the COT. However, the overall composition of the magmatic products older than 5.3 Ma as a function of their location along the back-arc COT allows us to distinguish four main groups (groups A, B, C, D in Table 2 and Figure 9). These groups correspond to the main morphostructural regions of the COT, i.e., Western Puna, Central Puna, Eastern Puna and Eastern Cordillera (Figure 9a). The composition of the rocks of the four groups lacks a clear subduction imprint (Ba/Nb < 40; Figure 9e), and indicates that different mantle and crustal domains were involved in magma generation, evident by the following points.

[28] 1. In the Western Puna, immediately behind the arc, group A basaltic-andesitic to dacitic magmas (Table 2 and Figure 9) formed the stratovolcanoes Tul-Tul, Del Medio and Pocitos. Volcanic rocks of these magmatic centers show particularly high Ba/Rb, Sr/Y and La/Yb ratios (Table 2) and have been interpreted as being derived from magmas generated by partial melting of a garnet-bearing lower crustal source and differentiated by MASH processes (melting-assimilation-storage-homogenization [*Matteini et al.*, 2002]), at the base of a thickened crust.

[29] 2. In the Central Puna, group B andesite and dacite magmas (Table 2 and Figure 9) erupted mainly as ignimbrites (Aguas Calientes center [*Petrinovic et al.*, 1999, 2010]). These centers show a peraluminous character (molar $Al_2O_3/CaO+Na_2O+K_2O > 1$) and high $^{87}Sr/^{86}Sr$, suggesting the involvement of the upper crust in the genesis of these magmas (Figures 9f and 9g).

[30] 3. In the Eastern Puna, group C andesitic rocks (Table 2 and Figure 9) produced stratovolcanoes, lava flows, domes and silicic ignimbrites. These products derive by mantle sources mixed with crustal melts [*Petrinovic et al.*, 1999, 2005; *Arnosio*, 2010].

[31] 4. In the Eastern Cordillera, group D andesitic magmas (Table 2 and Figure 9) were emplaced at 14–12 Ma (Las Burras). They show low Ba/Nb and La/Ta and relatively high Nb and low $^{87}Sr/^{86}Sr$ ratios, and formed by differentiation of magmas from a low $^{87}Sr/^{86}Sr$ lithospheric mantle that was rich in K, Rb, Th, with negligible crustal interaction [*Mazzuoli et al.*, 2008]. Conversely, the magmas

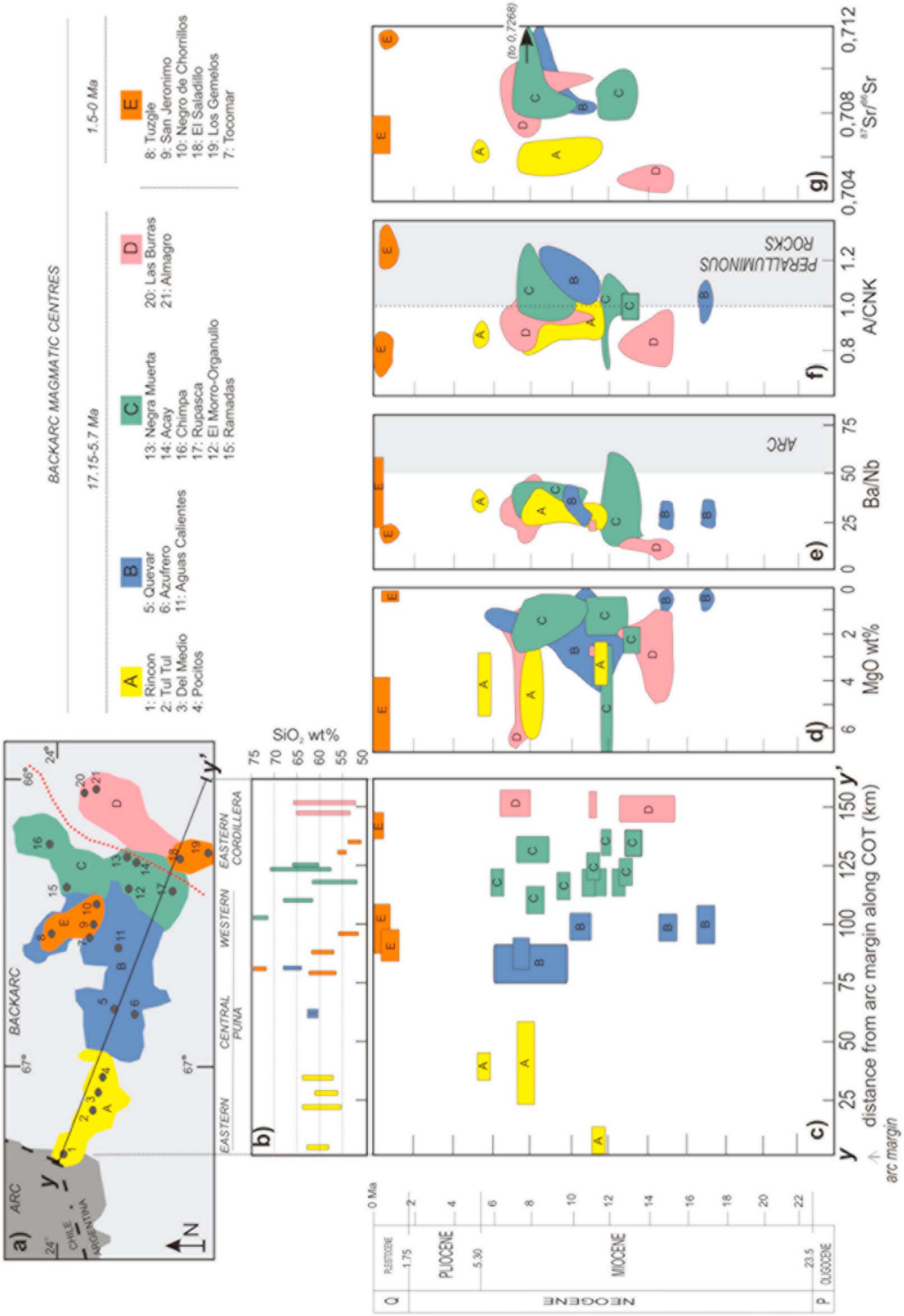

Figure 9. Time scale sketch map of the magmatic centers along the back-arc COT. (a) Areal distribution of magmatic groups A, B, C, D, and E (see also Table 2 and text) and list of related magmatic centers. (b) Variation of SiO_2 wt % versus along-COT distance from arc. (c) Available age data versus along-COT distance from the arc; each symbol includes error bars. (d) Age versus MgO wt %. (e) Age versus Ba/Nb, showing that the majority of back-arc rocks do not have arc characteristics. (f) Age versus A/CNK (molar $Al_2O_3/CaO+Na_2O+K_2O$, suggesting a crustal involvement in magma generation when > 1). (g) Age versus $^{87}Sr/^{86}Sr$. See the text for more details.

Table 2. Synthesis of the Main Volcanological, Petrological, Geochemical, and Age Data on the Magmatic Rocks of the Back-Arc COT[a]

Group	Location	magmatic Centers and Age[b] (Ma)	Field Characteristics and Rock Type	SiO_2 Range (wt %)	Sr/Y	Main Petrogenetic Models
A	Western Puna	1, Rincon (11.7); 2, Tul Tul (8.1–7.3); 3, Del Medio (5.7); 4, Pocitos (8.3)	basaltic andesite to dacite stratovolcanoes	55–64	25–80	melting of garnet-bearing lower crust (MASH)
B	Central Puna	5, Quevar (10, 8.6–7.5); 6, Azufrero (8.0); 11, Aguas Calientes (17.15–10.3)	andesite stratovolcanoes, andesite to dacite ignimbrite blankets, calderas	61–67	10–30	upper crust melting, shallow AFC
C	Eastern Puna	12, El Morro–Organullo (13–6); 13, Negra Muerta (9–7.3); 14, Acay monzonite (13); 15, Ramadas (8.5); 16, Chimpa (12); 17, Rupasca (11.4)	basaltic andesite to dacite lava domes and flows and stratovolcanoes, dacite ignimbrite blankets, rhyolite phreatomagmatic centers, calderas	52–74	15–50	shallow fractional crystallization and mixing of mantle- and crust-derived melts
D	Eastern Cordillera	20, Las Burras-Pancho Arias (15–12); 21, Almagro (11–6)	basaltic andesite to dacite lava domes and flows, cinder cones, intrusives	52–66	15–25	melting of lithospheric mantle sources, with a major change at 11 Ma, and moderate FC and AFC
E	Central Puna	7, Tocomar (1.5–0.55); 8, Tuzgle (0.5); 9, San Jeronimo (0.78); 10, Negro de Chorrillos (0.45)	rhyolite phreatomagmatic centers, shoshonite to latite effusive monogenetic centers	52–73	31–36	rhyolite, upper crust melting; shoshonite, low % partial melting of metasomatized lithospheric mantle
E	Eastern Cordillera	18, El Saladillo (<1); 19, Los Gemelos (0.035)	shoshonite effusive monogenetic centers	51–54	28–45	low % partial melting of metasomatized lithospheric mantle

[a]MASH, mixing-assimilation-storage-homogenization; FC, fractional crystallization; AFC, fractional crystallization and concomitant crustal assimilation.
[b]Error on ages between ± 0.2 and ± 0.9, except Quevar: 10 ± 2 Ma. References for group A: 1, *Gardeweg and Ramírez* [1987]; 2, 3, and 4, *Koukharsky and Munizaga* [1990] and *Matteini et al.* [2002]. References for group B: 5 and 6, *Olson and Gilzean* [1987] and *Petrinovic et al.* [1999]; 11, *Petrinovic et al.* [2010, and references therein]. References for group C: 12, *Petrinovic et al.* [1999] and *Arnosio et al.* [2005]; 13, *Riller et al.* [2001] and *Petrinovic et al.* [2005]; 14, *Haschke et al.* [2005]; 15, *Viramonte et al.* [1984]; 16, *Arnosio* [2010]; 17, *Petrinovic et al.* [1999]. References for group D: 20 and 21, *Sillitoe* [1977], *Hongn et al.* [2002], and *Mazzuoli et al.* [2008]. References for group E: 7, *Aquater* [1980] and *Petrinovic et al.* [1999, 2006]; 8, *Coira and Paris* [1981], and *Coira and Kay* [1993]; 9 and 10, *Aquater* [1980], *Deruelle* [1991], and *Kay et al.* [1994]; 18 and 19, *Guzmán et al.* [2006].

erupted after 12 Ma (Almagro) have relatively high $^{87}Sr/^{86}Sr$ (Figure 9g), despite an even more mafic composition. These magmas require an isotopically enriched, lithospheric mantle source [*Mazzuoli et al.*, 2008]. Apparently, the crust plays a minor role on magma generation in this back-arc sector during activity of the COT.

[32] Post 1.5 Ma volcanic activity differs from the previous activity. This younger volcanism occurs both in the Central Puna and Eastern Cordillera and forms an additional volcanic group, i.e., group E (Table 2 and Figure 9). This group includes (1) lavas with shoshonitic affinity, erupted from monogenetic centers [*Deruelle*, 1991; *Schreiber and Schwab*, 1991; *Petrinovic et al.*, 2006], (2) high-K andesites and shoshonites of the Tuzgle volcano [*Coira and Kay*, 1993] and (3) the rhyolitic, peraluminous tuffs of the Tocomar volcanic center. The shoshonitic rocks show 7–4 wt % MgO in the Central Puna (San Jeronimo and Negro de Chorrillos) and 9–7 wt % MgO in the Eastern Cordillera (Los Gemelos and El Saladillo; Figure 9d), a high content in compatible elements, high Ba/Nb (Figure 9e) and Sr isotopic ratios of 0.7064–0.7077 (Figure 9g). The generation of magmas with these chemical characteristics requires little partial melting of a metasomatized, garnet-bearing lithospheric mantle source [*Deruelle*, 1991; *Kay et al.*, 1994; *Petrinovic et al.*, 2005; *Guzmán et al.*, 2006]. Therefore, the eruption of the post–1.5 Ma shoshonites represents a threefold novelty, as (1) shoshonitic magmas were erupted first on the COT, (2) monogenetic centers occurred for the first time along the COT (Table 2), and (3) the same type of activity occurs both in the Puna and Eastern Cordillera, in contrast with the pre–5 Ma distinction in groups.

5. Discussion

5.1. Interpretation of the Remote Sensing, Geological, and Structural Data

[33] The distribution of the lineaments and the major known fault systems on the back-arc COT shows an overall good spatial correlation, in terms of location and orientation, suggesting that most of the lineaments are due to faulting (Figure 2). Most faults trend ~N–S and ~NW–SE, with the latter ones occurring in the central portion of the COT and spatially associated with volcanic centers (Figure 2). Moreover, the geometric continuity between part of the ~N–S and ~NW–SE fault systems (Figure 2) suggests that part of these faults are coeval. These relationships are supported by the structural field data. Specifically, fault crosscutting relationships show that ~N–S and ~NW–SE systems are in part coeval, even though a significant part of the ~NW–SE systems postdate the ~N–S trending regional structures. Also, the age of the sedimentary and volcanic deposits, which are affected by the ~NW–SE striking faults, points to significant late Neogene to Quaternary tectonic activity (Table 1). Quaternary activity of the COT is consistent with seismicity in this area, indicating left-lateral motion on the COT [*Schurr et al.*,

1999]. Shortening in the Puna, as due to the activity of ~N–S trending reverse faults, terminated mostly prior to ~10 Ma [*Cladouhos et al.*, 1994; *Coutand et al.*, 2001, and references therein; *Müller et al.*, 2002], while shortening in the Eastern Cordillera is ongoing [*Marrett et al.*, 1994; *Marrett and Strecker*, 2000]. These considerations suggest that structures of the back-arc COT have been active from the Miocene to the Present. This age interval is broadly consistent with that of magmatic activity along the back-arc COT (Figure 9), pointing to a genetic relationship between magmatism and deformation.

[34] The ~NW–SE trending COT faults dip steeply and adhere to an overall transtensive kinematic regime (Figures 5 and 7). Therefore, the kinematics of the back-arc COT, as defined in this study, suggests that the other NW–SE trending structures in the Central Andes (Figure 1) are also characterized by left-lateral transtension.

[35] If we consider our structural data to be representative of the entire back-arc COT, they may allow us to make the following points.

[36] 1. The back-arc COT, in addition to a magmatic and geomorphologic characterization, has a structural expression, which corresponds to a major left-lateral transtensive fault zone. This supports previous tectonic models and structural results on individual portions of the COT [*Riller et al.*, 2001; *Ramelow et al.*, 2006; *Petrinovic et al.*, 2006].

[37] 2. The likely Miocene to Quaternary activity of the COT structures crudely overlaps in time with the Miocene to Quaternary activity of the magmatic centers. As it will be discussed in section 5.2, the observed transtensive motion along the COT may provide favorable conditions for the rise and emplacement of magma.

5.2. Structural Control on Magmatism of the COT

[38] Strike-slip and transtensive fault kinematics are responsible for localized areas of horizontal extension (forming pull-apart basins, tension gashes, releasing bends), which may provide the space required for the storage and transport of magma [e.g., *Bellier et al.*, 1999; *Lavenu and Cembrano*, 1999; *Garcia Palomo et al.*, 2004, and references therein]. Strike-slip and extensional structures at the surface require equivalent kinematic regimes at depth in the crust, evident by the syntectonic emplacement of plutons, constituting the magma chambers of arc volcanoes [e.g., *Morand*, 1992; *Moreau et al.*, 1994; *Vigneresse*, 1995; *Castro and Fernández*, 1998; *Gibbons and Moreno*, 2002; *Wagner et al.*, 2006]. Therefore, strike-slip and transtensive structures may well control magma transport and emplacement in arcs at shallower and deeper crustal levels.

[39] The importance of local extension for localizing magmatism along the COT is supported by our structural field evidence, indicating that orogen-parallel extension is focused in the central COT corridor (Figure 8). Also, the tectonomagmatic relationships described above apply to the 21 main magmatic centers of the COT (Figures 2 and 9). Information on the structural control is available for 13 magmatic centers, 9 of which are located in the Puna and 4 in the Eastern Cordillera. Studies on the 9 centers in the Puna (Tul-Tul, Del Medio, Pocitos, Tocomar, Negro de Chorillos, San Jeronimo, Aguas Calientes, Negra Muerta and Chimpa; Figure 2) suggest that magmatism was controlled by the activity of COT-parallel faults and/or related extensional structures [*Petrinovic*, 1999; *Riller et al.*, 2001; *Arnosio*, 2002; *Matteini et al.*, 2002; *Ramelow et al.*, 2006; *Petrinovic et al.*, 2005, 2006, 2010; *Petrinovic and Colombo Piñol*, 2006]. Conversely, the development of the 4 centers in the Eastern Cordillera (El Saladillo, Los Gemelos, Las Burras, Almagro) appears to be also controlled by the activity of N–S trending transpressive faults [*Guzmán et al.*, 2006; *Acocella et al.*, 2007; *Mazzuoli et al.*, 2008]. Therefore, activity of magmatic centers located on the Puna may be chiefly controlled by COT-related structures, whereas the activity of the centers within the Eastern Cordillera is also controlled by the ~N–S fault systems. This behavior reflects likely the deep structure of crust underlying the Puna and the Eastern Cordillera. In particular, the Puna is characterized by a relatively lower spatial density of ~N–S trending regional faults, whereas the Eastern Cordillera appears pervasively controlled by the ~N–S striking faults, accomplishing basement-involved thrusting and significantly larger shortening magnitudes than the Puna [*Kley and Monaldi*, 2002; *Müller et al.*, 2002; *Acocella et al.*, 2007, and references therein]. Independently of these morphotectonic domains, strike-slip faults (NW–SE striking transtension zones and, subordinately, ~N–S striking transpressive fault zones), seem to provide ideal conditions for localizing magmatism along the COT.

[40] In broader terms, our data from the back-arc COT show that there is a spatial correlation between the frequency of the lineaments and faults (calculated from Figure 2 and shown in Figure 10b) and the areal distribution (in km^2) of the magmatic deposits (calculated from Figure 2 and shown in Figure 10c), with a peak in the central part. Specifically, the central portion of the COT is the widest; to the east and to the west, the spatial density and length of faults decrease significantly (Figure 10). If we consider the areal distribution of the magmatic deposits as indicative of their volume, this correspondence implies that most of the magma was erupted in the tectonically more developed central portion of the back-arc COT.

[41] A correlation between the overall geometry of the COT and the composition of its magmatic rocks is also apparent from our data. Geochemical data from the 17–5 Ma COT magmatic centers show a marked difference in composition between the magmas spatially associated with the central part of the COT and those found toward its eastern and western extremities (Table 2 and Figures 9 and 10). The latter include mantle-derived magmas that are moderately differentiated in crustal reservoirs. Conversely, magmatic rocks from the central COT are mostly derived from evolved magmas (dacite-ryholite), with a clear component from upper crust melting (Table 2 and Figure 10d, continuous lines). A similar trend, although with lower volumes of erupted magmas, is also shown by the volcanic activity in the last 1.5 Ma (Figure 10d, dashed lines): rhyolites and high-K andesites accompany shoshonites in the central back-arc COT, while only shoshonites occur in the Eastern Cordillera. It is also noteworthy that, in agreement with this evidence, post–1.5 Ma shoshonites in the Central Puna show a moderate degree of differentiation by fractional crystallization during magma ascent in the crust, whereas shoshonites in the Eastern Cordillera show more primitive chemical

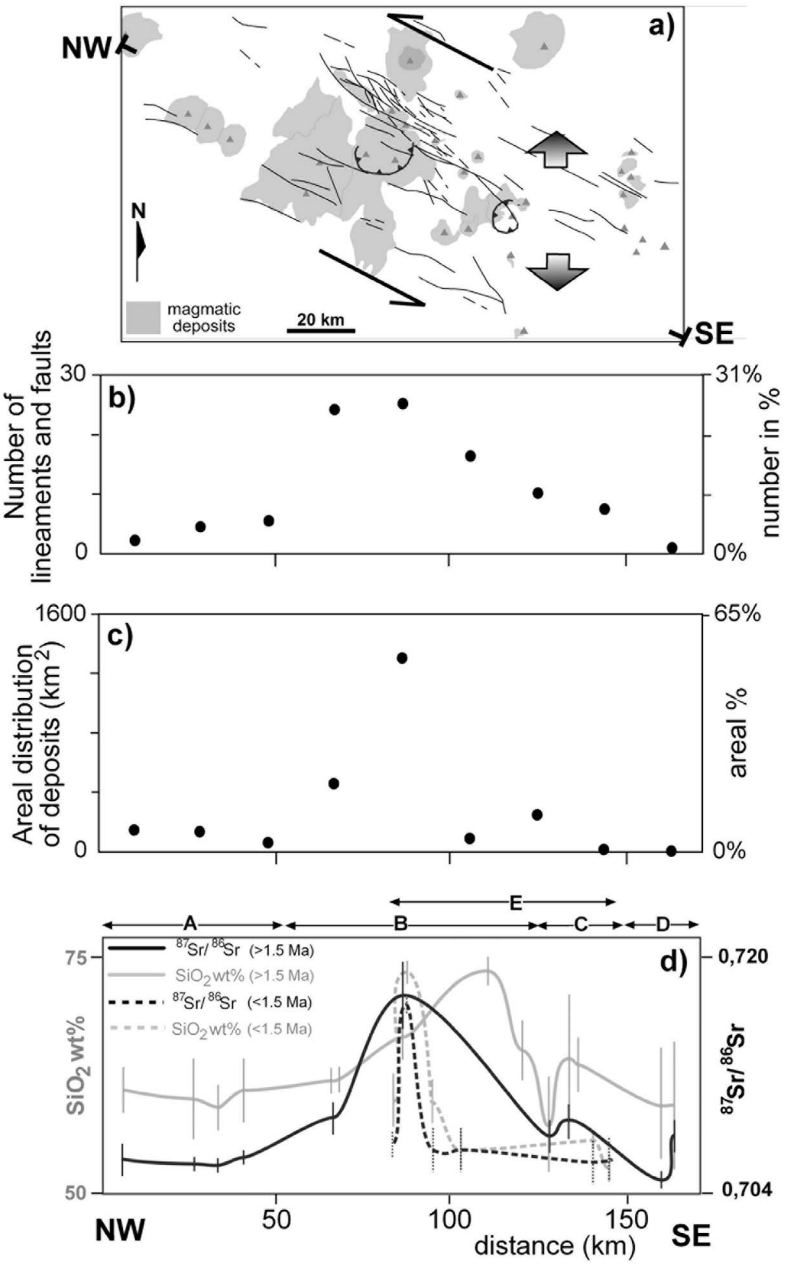

Figure 10. Summary of the main tectonomagmatic features of the back-arc part of the COT. (a) Sketch reporting the location (triangles) and extent (in gray) of the main magmatic centers and the main lineaments and faults (from Figure 2). The simplified kinematics of the COT systems, consisting of left-lateral transtension with an orogen-parallel extension, is also highlighted. (b) Frequency distribution of the main lineaments and faults (from Figure 2, here calculated with a sampling frequency of 20 km) as a function of along-COT distance (see trace of profile in Figure 10a). (c) Areal distribution (in km^2) of the magmatic deposits as a function of along-COT distance (calculated with the same sampling frequency of 20 km as in Figure 10b). The mean error is < 20%. (d) SiO_2 wt % and $^{87}Sr/^{86}Sr$ ratio of the magmatic products as a function of along-COT distance from arc (see trace of profile in Figure 10a); vertical lines indicate the range of values for each magmatic center. The groups A to E of Figure 9 are also highlighted. In general, the most fractured central part of the COT shows the highest SiO_2 and $^{87}Sr/^{86}Sr$ values, suggesting an important role of the COT structures on enhancing magmatism at crustal levels. See text for further details.

characteristics (e.g., Cr < 100 ppm, 7–4 wt % MgO, against Cr > 400 ppm, 9–7 wt % MgO [*Deruelle*, 1991; *Guzmán et al.*, 2006]). We propose that the magmas from the central COT are related to a more permeable, possibly tectonically dilated, zone [e.g., *Gudmundsson*, 2000], providing space for the storage of magma in the crust and allowing for its differentiation and enhancing interaction with crustal melts. This can also account for the presence of collapse calderas, which are the surface expression of large and long-lived magmatic centers, in the central COT. Conversely, at the western and eastern back-arc COT, the contribution of the upper crust to magma petrogenesis is limited. This points to a diminished capacity of magma storage in the upper crust, possibly resulting from a lower permeability brought about by lower magnitudes of horizontal extension (dilation).

[42] Volcanic rocks from the area between the Central Puna and Eastern Cordillera (group C rocks; Figure 9) show characteristics of both evolved and primitive magma sources. The continental crust seems to be the main source for the magmas in the Central Puna, whereas the lithospheric mantle seems to be the dominant source for the magmas in the Eastern Cordillera. Accordingly, the Negra Muerta volcanic complex (group C rocks; Figure 9), lies in an intermediate position, with respective magmatic characteristics, i.e., mantle- and crust-derived magmas.

[43] Post–1.5 Ma magmatism, such as in the Tocomar area, is also bimodal and corroborates, at a local scale, our hypothesis of dilation-controlled magmatic characteristics. The Tocomar rhyolitic magmas are related to normal faults, suggesting storage at shallow crustal level. By contrast, shoshonitic magmas at San Jeronimo are associated with strike-slip faults, pointing to rapid magma ascent from the base of the crust [*Petrinovic et al.*, 2006].

[44] In summary, the diagrams in Figure 10 suggest that the tectonically more developed (Figure 10b) central part of the back-arc COT was associated with the eruption of large magma volumes (Figure 10c) and corresponds to large volumes of magma stored in the crust (Figure 10d). Similar relationships, between magma volumes and composition and horizontal extension of crust, have been previously suggested for convergent and divergent plate boundaries. For example, at the Peruvian convergent margin, magma storage has been attributed to larger magnitudes of horizontal extension [*Grocott et al.*, 1994; *McNulty et al.*, 1998]. Similarly, the southern Main Ethiopian Rift, which features lower horizontal extension magnitudes, is dominated by mafic volcanic rocks, whereas the central Rift, which is characterized by larger magnitudes of extension, shows widespread bimodal volcanism, with felsic magmas from crustal reservoirs [*Hayward and Ebinger*, 1996; *Ebinger and Casey*, 2001; *Corti*, 2009].

5.3. The Availability of Magma at Depth

[45] In this study we offer an explanation for the structural influence on magmatic activity along the COT, as related to transtensive tectonism. We also briefly address the source of magma at depth below the COT and located at distances of nearly 300 km to the east of the active volcanic arc.

[46] The genesis of magma to explain pre–12 Ma back-arc magmatism has been attributed to steepening of the subducting slab [*Isacks*, 1988; *Kay et al.*, 1999] and thus replacement of the slab by asthenosphere. This change in thermal regime may well have provided the initial sources for the mantle- and crust-derived melts at the central COT. Subsequent back-arc magmatism, however, occurred during lithospheric thickening. In this framework, delamination of the thickened and weakened lithospheric lid has been repeatedly invoked to explain the local rise of hotter asthenosphere and magma production in the back arc of Central Andes [*Kay and Kay*, 1993; *Yuan et al.*, 2002]. Delamination of lithospheric mantle may explain the initiation and termination of magmatic pulses in other back-arc settings, such as the Sierra Nevada [*Elkins-Tanton and Grove*, 2003]. In the Central Andes, delamination was first suggested for the most recent (<2 Ma) back-arc magmatism in the Puna Plateau [e.g., *Kay et al.*, 1994]. However, recent age determinations of back-arc magmatic products indicate that the magmatic pulse which may be linked to delamination in the southern Puna, at 26°S, had its peak at about 5 Ma [*Risse et al.*, 2008; *Gioncada et al.*, 2010]. In addition, other studies have recently suggested that delamination may have been the cause for magma generation below the Altiplano-Puna Volcanic Complex, immediately to the north of the COT, during 12–10 Ma [*McQuarrie et al.*, 2005; *De Silva et al.*, 2006]. These repeated magmatic events in contiguous portions of the Central Andes suggest the occurrence of episodic, or piecemeal-type, delamination processes [*McQuarrie et al.*, 2005], of which the currently detached lithosphere slab below the Puna [*Schurr et al.*, 2006] is probably the last episode.

[47] As far as the possible effects of any delamination on the COT magmatic belt are concerned, our overview highlights at least two main periods which require changes in the mantle melting regions, which may be consistent with the previously proposed piecemeal lithospheric delamination. The first period, at 12–11 Ma, is characterized by the abrupt change in the mantle-derived magma composition with the Almagro volcanic rocks, in the Eastern Cordillera [*Mazzuoli et al.*, 2008]. This event coincides with the peak of ignimbrite activity in the central COT sector and the spreading of magmatic activity to the entire COT belt (Figure 9), suggesting intense magma generation in the back arc and a connection with the ~12 Ma Altiplano-Puna ignimbrite flare-up [*McQuarrie et al.*, 2005]. The second period is younger than 1.5 Ma and associated with the eruption of shoshonitic magmas that may well be related to the latest delamination pulse, also imaged by tomographic data [*Kay et al.*, 1994; *Schurr et al.*, 2006].

[48] It appears that the occurrence of magmatism in the back arc of the Central Andes may have been related to different processes, acting at different times and scales. At the regional scale, previous studies suggest that the availability of magma below the back arc of Central Andes may be related to slab steepening, during early middle Miocene [*Isacks*, 1988; *Kay et al.*, 1999] and, most likely, delamination, during middle Miocene to Quaternary, responsible for the repeated waxing and waning magma generation pulses [*McQuarrie et al.*, 2005; *Risse et al.*, 2008; *Mazzuoli et al.*, 2008]. Once the magma was generated, its rise and any storage in the crust occurred by means of ~NW–SE trending transtensive structures. Occasionally, as in the Eastern Cor-

dillera, ~N–S trending transpressive regional systems may have further enhanced the rise and emplacement of magma [*Guzmán et al.*, 2006; *Mazzuoli et al.*, 2008].

6. Conclusions

[49] This study allows for highlighting the following points.

[50] 1. Our structural data demonstrate that the back-arc COT consists of subparallel ~NW–SE trending fault systems, with an overall left-lateral transtensive motion. COT faults formed in Miocene to Quaternary times, are partly coeval with magmatism, and partly postdate the activity of N–S striking faults. Transtensive structures create areas of localized extension and provide favorable conditions for the ascent and storage of magma.

[51] 2. COT magmatism on the Puna appears to be controlled by ~NW–SE trending structures, whereas magmatism in the Eastern Cordillera is also controlled by the activity of the N–S regional structures.

[52] 3. The most evolved magmas, with a clear crustal component, were erupted along the central part of the back-arc COT, where upper crustal faults display higher spatial density. Mantle-derived mafic rocks, and primitive products, however, seem to have been directly fed by the mantle and are mainly found toward the COT termini, where faults are less prevalent. The central COT is also characterized by the largest erupted magma volumes. This implies larger magma production rates and suggests that larger dilation magnitudes of the central COT favor the ascent of magma and the formation of crustal reservoirs.

[53] 4. The occurrence of magmatism in the back arc of the Central Andes seems related to different processes, acting at different scales and levels. According to previous studies, at the regional scale, magma generation may be largely related to episodic lithospheric delamination. In the last 17 Ma, during the formation of the COT magmatic belt, we highlight two periods, at 12–11 Ma and < 1.5 Ma, which may be related to important changes at the lithospheric scale.

[54] **Acknowledgments.** Pablo Cavalieri, Eugenia Franzoni, Massimo Matteini, and Julieta Omarini provided enthusiastic help and expert advice during the field work. O. Galland and an anonymous reviewer provided helpful comments. This work was carried out in the framework of the scientific convention between Pisa (Italy) and Salta (Argentina) Universities. The research was supported by the Consejo Nacional de Investigaciones Cientificas y Técnicas (CONICET-Agencia, Argentina, PICT 0745-) and the Consejo de Investigaciones de la Universidad Nacional de Salta (CIUNSA, Argentina, project 1861), the Italian Ministry of University and Research (MIUR-PRIN 2003 project), and the Natural Sciences and Engineering Research Council of Canada. Structural data partly elaborated with DAISY software (kind permission of F. Salvini, Roma TRE).

References

Acocella, V., and F. Funiciello (2010), Structural control of arc volcanism and related kinematic setting: An overview, *Earth Planet. Sci. Lett.*, *289*, 43–53, doi:10.1016/j.epsl.2009.10.027.

Acocella, V., L. Vezzoli, R. Omarini, M. Matteini, and R. Mazzuoli (2007), Kinematic variations across Eastern Cordillera at 24°S (Central Andes): Tectonic and magmatic implications, *Tectonophysics*, *434*, 81–92, doi:10.1016/j.tecto.2007.02.001.

Acocella, V., T. Yoshida, R. Yamada, and F. Funiciello (2008), Structural control on late Miocene to Quaternary volcanism in the NE Honshu arc, Japan, *Tectonics*, *27*, TC5008, doi:10.1029/2008TC002296.

Alaniz-Alvarez, S. A., Á. F. Nieto-Samaniego, and L. Ferrari (1998), Effect of strain rate in the distribution of monogenetic and polygenetic volcanism in the Transmexican volcanic belt, *Geology*, *26*, 591–594, doi:10.1130/0091-7613(1998)026<0591:EOSRIT>2.3.CO;2.

Allmendinger, R. W., V. A. Ramos, T. E. Jordan, M. Palma, and B. L. Isacks (1983), Paleogeography and Andean structural geometry, northwest Argentina, *Tectonics*, *2*, 1–16, doi:10.1029/TC002i001p00001.

Allmendinger, R. W., T. E. Jordan, S. M. Kay, and B. L. Isacks (1997), The evolution of the Altiplano-Puna Plateau of the Central Andes, *Annu. Rev. Earth Planet. Sci.*, *25*, 139–174, doi:10.1146/annurev.earth.25.1.139.

Angelier, J., and J. Goguel (1979), Sur une méthode simple de détermination des axes principaux des contraintes pour une population de failles, *C. R. Acad. Sci. Hebd. Seances Acad. Sci., Ser. D*, *288*, 307–310.

Aquater (1980), Exploracion geotermica en el area del Cerro Tuzgle, Provincia de Jujuy, Republica Argentina, estudio de prefactibilidad inedito, 123 pp., Secr. de Miner. de la Prov. de Jujuy, Argentina, Jujuy, Argentina.

Arnosio, J. M. (2002), Volcanismo, geoquímica y petrología del volcán Chimpa (24° LS–66° LO) provincia de Salta, República Argentina, Ph.D. thesis, 176 pp., Univ. Nac. de Salta, Salta, Argentina.

Arnosio, J. M. (2010), Evidencia textural y geoquímica de mezcla de magmas en el Volcan Chimpa, Puna Salteña, *Asoc. Geol. Argent. Rev.*, *66*, 251–268.

Arnosio, J. M., V. Marmol, and R. Becchio (2005), Estratigrafia volcanica y evolucion del centro volcanico El Morro (24°17′S–66°15′O), Puna Salteña, in *Actas XVI Congreso Geologico Argentino, la Plata, 2005*, vol. 1, pp. 859–866, Asoc. Geol. Argentina, Buenos Aires.

Bellier, O., H. Bellon, M. Sebrier, P. Sutanto, and R. C. Maury (1999), K-Ar age of the Ranau tuffs: Implications for the Ranau caldera emplacement and slip-partitioning in Sumatra (Indonesia), *Tectonophysics*, *312*, 347–359, doi:10.1016/S0040-1951(99)00198-5.

Blasco, G., E. O. Zappettini, and F. Hongn (1996), Hoja geológica 2566-1, San Antonio de los Cobres, Programa Nac. de Carteas Geol. de la Repub. Argentina, Dir. Nac. del Serv. Geol., Buenos Aires.

Byerlee, J. D. (1968), Brittle-ductile transition in rocks, *J. Geophys. Res.*, *73*, 4741–4750, doi:10.1029/JB073i014p04741.

Caffe, P. J., R. B. Trumbull, B. L. Coira, and R. L. Romer (2002), Petrogenesis of early Neogene magmatism in the northern Puna: Implications for magma genesis and crustal processes in the central Andean plateau, *J. Petrol.*, *43*, 907–942, doi:10.1093/petrology/43.5.907.

Castro, A., and C. Fernández (1998), Granite intrusion by externally induced growth and deformation of the magma reservoir, the example of the Plasenzuela pluton, Spain, *J. Struct. Geol.*, *20*, 1219–1228, doi:10.1016/S0191-8141(98)00056-X.

Chernicoff, C. J., J. P. Richards, and E. O. Zappettini (2002), Crustal lineament control on magmatism and mineralization in northwestern Argentina: Geological, geophysical, and remote sensing evidence, Ore Geol. *Rev.*, *21*, 127–155.

Cladouhos, I. T., R. W. Allmendinger, B. Coira, and E. Farrar (1994), Late Cenozoic deformations in the Central Andes: Fault kinematics from the northern Puna, northwest Argentina and southwest Bolivia, *J. South Am. Earth Sci.*, *7*, 209–228, doi:10.1016/0895-9811(94)90008-6.

Coira, B., and S. Kay (1993), Implication of Quaternary volcanism at Cerro Tuzgle for crustal and mantle evolution of the Puna Plateau, Central Andes, Argentina, Contrib. Mineral. *Petrol.*, *113*, 40–58, doi:10.1007/BF00320830.

Coira, B., and G. Paris (1981), Estratigrafia volcanica del area del Cerro Tuzgle, Provincias de Jujuy y Salta, in *VIII Congreso Geológico Argentino, Actas*, vol. 3, 659–671, Asoc. Geol. Argentina, San Luis, Argentina.

Cole, J. W. (1990), Structural control and origin of volcanism in the Taupo volcanic zone, New Zealand, *Bull. Volcanol.*, *52*, 445–459, doi:10.1007/BF00268925.

Corti, G. (2009), Continental rift evolution: From rift initiation to incipient break-up in the Main Ethiopian Rift, East Africa, *Earth Sci. Rev.*, *96*, 1–53, doi:10.1016/j.earscirev.2009.06.005.

Corti, G., E. Carminati, F. Mazzarini, and M. O. Garcia (2005), Active strike-slip faulting in El Salvador, Central America, *Geology*, *33*, 989–992, doi:10.1130/G21992.1.

Coutand, I., P. R. Cobbold, M. de Urreiztieta, P. Gautier, A. Chauvin, D. Gapais, E. A. Rossello, and O. López-Gamundí (2001), Style and history of Andean deformation, Puna plateau, northwestern Argentina, *Tectonics*, *20*, 210–234, doi:10.1029/2000TC900031.

Deeken, A., E. R. Sobel, I. Coutand, M. Haschke, U. Riller, and M. R. Strecker (2006), Development of the southern Eastern Cordillera, NW Argentina, constrained by apatite fission track thermochronology: From Early Cretaceous extension to middle Miocene shortening, *Tectonics*, *25*, TC6003, doi:10.1029/2005TC001894.

Deruelle, B. (1991), Petrology of Quaternary shoshonitic lavas of northwestern Argentina, in *Andean Magmatism and Its Tectonic Setting*, edited by R. S. Harmon and C. W. Rapela, *Spec. Pap. Geol. Soc. Am.*, *256*, 201–217.

De Silva, S., G. Zandt, R. Trumbull, J. G. Viramonte, G. Salas, and N. Jiménez (2006), Large ignimbrite eruptions and volcano-tectonic depressions in

the Central Andes: A thermomechanical perspective, in *Mechanism of Activity and Unrest at Large Calderas*, edited by C. Troise, G. De Natale, and C. R. Kilburn, *Geol. Soc. Spec. Publ.*, *269*, 47–63.

Ebinger, C. J., and M. Casey (2001), Continental breakup in magmatic provinces: An Ethiopian example, *Geology*, *29*, 527–530, doi:10.1130/0091-7613(2001)029<0527:CBIMPA>2.0.CO;2.

Elger, K., O. Oncken, and J. Glodny (2005), Plateau-style accumulation of deformation: Southern Altiplano, *Tectonics*, *24*, TC4020, doi:10.1029/2004TC001675.

Elkins-Tanton, L. T., and T. L. Grove (2003), Evidence for deep melting of hydrous metasomatized mantle: Pliocene high-potassium magmas from the Sierra Nevadas, *J. Geophys. Res.*, *108*(B7), 2350, doi:10.1029/2002JB002168.

Galland, O., E. Hallot, P. R. Cobbold, G. Ruffet, and J. de Bremond d'Ars (2007), Volcanism in a compressional Andean setting: A structural and geochronological study of Tromen volcano (Neuquén province), Argentina, *Tectonics*, *26*, TC4010, doi:10.1029/2006TC002011.

Garcia Palomo, A., J. L. Macias, and J. M. Espíndola (2004), Strike-slip faults and K-alkaline volcanism at El Chichón volcano, southeastern Mexico, *J. Volcanol. Geotherm. Res.*, *136*, 247–268, doi:10.1016/j.jvolgeores.2004.04.001.

Gardeweg, M., and C. F. Ramírez (1987), La Pacana Caldera and the Atana Ignimbrite—A major ash-flow and resurgent caldera complex in the Andes of northern Chile, *Bull. Volcanol.*, *49*, 547–566, doi:10.1007/BF01080449.

Gibbons, W., and T. Moreno (2002), Tectonomagmatism in continental arcs: Evidence from the Sark arc complex, *Tectonophysics*, *352*, 185–201, doi:10.1016/S0040-1951(02)00196-8.

Gioncada, A., N. Hauser, M. Matteini, R. Mazzuoli, and R. Omarini (2006), Mingling and mixing features in basaltic andesites of the Eastern Cordillera (Central Andes, 24°S): A petrographic and microanalytical study, *Period. Mineral.*, *75*, 127–139.

Gioncada, A., L. Vezzoli, R. Mazzuoli, R. Omarini, P. Nonnotte, and H. Guillou (2010), Pliocene intraplate-type volcanism in the Andean foreland at 26°10′S, 64°40′W (NW Argentina): Implications for magmatic and structural evolution of the Central Andes, *Lithosphere*, *2*, 153–171, doi:10.1130/L81.1.

Goddard, P., J. J. Willson, S. Couch, and J. Viramonte (1999), The evolution of El Quevar volcanic complex, Salta Province, Argentina, in *XIV Congreso Geológico Argentino*, vol. 2, pp. 225–227, Asoc. Geol. Argentina, Salta, Argentina.

Grocott, J., M. Brown, R. D. Dallmeyer, G. K. Taylor, and P. J. Treloar (1994), Mechanisms of continental growth in extensional arcs: An example from the Andean plate-boundary zone, *Geology*, *22*, 391–394, doi:10.1130/0091-7613(1994)022<0391:MOCGIE>2.3.CO;2.

Gudmundsson, A. (2000), Fracture dimensions, displacements and fluid transport, *J. Struct. Geol.*, *22*, 1221–1231, doi:10.1016/S0191-8141(00)00052-3.

Gudmundsson, A., T. H. Simmenes, B. Larsen, and S. L. Philipp (2010), Effects of internal structure and local stresses on fracture propagation, deflection, and arrest in fault zones, *J. Struct. Geol.*, *32*, 1643–1655, doi:10.1016/j.jsg.2009.08.013.

Guzmán, S. R., I. A. Petrinovic, and J. A. Brod (2006), Pleistocene mafic volcanoes in the Puna-Cordillera Oriental boundary, NW-Argentina, *J. Volcanol. Geotherm. Res.*, *158*, 51–69, doi:10.1016/j.jvolgeores.2006.04.014.

Haschke, M., A. Deeken, N. Insel, E. Sobel, M. Grove, and A. K. Schmitt (2005), Growth pattern of the Andean Puna plateau by apatite fission track apatite (U-Th)/He, K-feldspar $^{40}Ar/^{39}Ar$, and zircon U-Pb geochronology, in *6th International Symposium on Andean Geodynamics, Barcelona*, edited by Institut de Recherche Pour le Développement, pp. 360–363, Inst. de Rech. Pour le Dev., Paris.

Hayward, N. J., and C. J. Ebinger (1996), Variation in the along-axis segmentation of the Afar Rift system, *Tectonics*, *15*, 244–257, doi:10.1029/95TC02292.

Hindle, D., J. Kley, O. Oncken, and S. Sobolev (2005), Crustal balance and crustal flux from shortening estimates in the Central Andes, *Earth Planet. Sci. Lett.*, *230*, 113–124, doi:10.1016/j.epsl.2004.11.004.

Hongn, F., and U. Riller (2007), Tectono-magmatic evolution of the western margin of Gondwana inferred from syntectonic emplacement of Paleozoic granitoid plutons in NW-Argentina, *J. Geol.*, *115*, 163–180, doi:10.1086/510644.

Hongn, F. D., and R. E. Seggiaro (2001), Hoja geológica 2566-III, Cachi, scale 1:250.000, *Bol. 248*, SEGEMAR, Buenos Aires.

Hongn, F. D., J. M. Tubia, A. Aranguren, and R. Mon (2002), La monzodiorita Las Burras: Un pluton miocenico en el batolito de Tastil, Cordillera Oriental Argentina, in *Actas del XV Congreso Geologico Argentino, 2002*, vol. 2, pp. 128–133, Asoc. Geol. Argentina, Buenos Aires.

Isacks, B. L. (1988), Uplift of the central Andean plateau and bending of the Bolivian orocline, *J. Geophys. Res.*, *93*, 3211–3231.

Jordan, T. E., and R. N. Alonso (1987), Cenozoic stratigraphy and basin tectonics of the Andes mountains, 20°–28° south latitude, *AAPG Bull.*, *71*, 49–64.

Kay, R. W., and S. M. Kay (1993), Delamination and delamination magmatism, *Tectonophysics*, *219*, 177–189, doi:10.1016/0040-1951(93)90295-U.

Kay, S. M., B. Coira, and J. Viramonte (1994), Young mafic back arc volcanic rocks as indicators of continental lithospheric delamination beneath the Argentine Puna Plateau, Central Andes, *J. Geophys. Res.*, *99*, 24,323–24,339, doi:10.1029/94JB00896.

Kay, S. M., C. Mpodozis, and B. Coira (1999), Magmatism, tectonism, and mineral deposits of the Central Andes (22°–33°S latitude), in *Geology and Ore Deposits of the Central Andes*, edited by B. Skinner, *Spec. Publ. Soc. Econ. Geol.*, *7*, 27–59.

Kley, J. (1996), Transition from basement-involved to thin-skinned thrusting in the Cordillera Oriental of southern Bolivia, *Tectonics*, *15*, 763–775, doi:10.1029/95TC03868.

Kley, J., and C. R. Monaldi (1998), Tectonic shortening and crustal thickness in the Central Andes: How good is the correlation?, *Geology*, *26*, 723–726, doi:10.1130/0091-7613(1998)026<0723:TSACTI>2.3.CO;2.

Kley, J., and C. R. Monaldi (2002), Tectonic inversion in the Santa Barbara System of the central Andean foreland thrust belt, northwestern Argentina, *Tectonics*, *21*(6), 1061, doi:10.1029/2002TC902003.

Koukharsky, M., and F. Munizaga (1990), Los volcanes: Guanaquero, Chivinar Tul Tul, Del Medio y Pocitos, provincial de Salta, Argentina: Litologías y edades K/Ar, in *XI Congreso Geológico Argentino*, vol. 1, pp. 64–67, Asoc. Geol. Argentina, San Juan, Argentina.

Kraemer, B., D. Adelmann, M. Alten, W. Schnurr, K. Erpenstein, E. Kiefer, P. van den Bogaard, and K. Görler (1999), Incorporation of the Paleogene foreland into the Neogene Puna plateau: The Salar de Antofalla area, NW Argentina, *J. South Am. Earth Sci.*, *12*, 157–182, doi:10.1016/S0895-9811(99)00012-7.

Krallmann, A. (1994), Petrographische und geochemische untersuchungen an jungen, basichen vulkaniten im bereich des Calama–Olacapato–El Toro lineaments östlich der vulkankette, NW Argentinien, *Clausthaler Geowiss. Diss. 160*, 79 pp., Inst. Fur Geol. und Palaontol., Stuttgart, Germany.

Lavenu, A., and J. Cembrano (1999), Compressional- and trasnpressional-stress pattern for Pliocene and Quaternary brittle deformation in fore arc and intra-arc zones (Andes of central and southern Chile), *J. Struct. Geol.*, *21*, 1669–1691, doi:10.1016/S0191-8141(99)00111-X.

Maffione, M., F. Speranza, and C. Faccenna (2009), Bending of the Bolivian orocline and growth of the central Andean plateau: Paleomagnetic and structural constraints from the Eastern Cordillera (22–24°S, NW Argentina), *Tectonics*, *28*, TC4006, doi:10.1029/2008TC002402.

Marrett, R., and M. R. Strecker (2000), Response of intracontinental deformation in the Central Andes to the late Cenozoic reorganization of South American Plate motions, *Tectonics*, *19*, 452–467, doi:10.1029/1999TC001102.

Marrett, R. A., R. W. Allmendinger, R. N. Alonso, and R. Drake (1994), Late Cenozoic tectonic evolution of the Puna Plateau and adjacent foreland, northwestern Argentine Andes, *J. South Am. Earth Sci.*, *7*, 179–207, doi:10.1016/0895-9811(94)90007-8.

Matteini, M. (2001), Evolución petrológica, geoquímica y evaluacion de los mecanismos eruptivos en los complejos volcanicos Tul-Tul, Del medio y Pocitos, Puna Argentina: El rol del lineamiento Calama-Olacapato-El Toro, Ph.D. thesis, 176 pp., Univ. Nac. de Salta, Salta, Argentina.

Matteini, M., R. Mazzuoli, R. Omarini, R. A. F. Cas, and R. Maas (2002), Geodynamical evolution of the Central Andes at 24°S as inferred by magma composition along the Calama–Olacapato–El Toro transversal volcanic belt, *J. Volcanol. Geotherm. Res.*, *118*, 205–228, doi:10.1016/S0377-0273(02)00257-3.

Mazzuoli, R., et al. (2008), Miocene magmatism and tectonics in the easternmost sector of the Calama–Olacapato–El Toro fault system in Central Andes at ~24°S: Insights into the evolution of the Eastern Cordillera, *Geol. Soc. Am. Bull.*, *120*, 1493–1517, doi:10.1130/B26109.1.

McNulty, B., D. Farber, G. S. Wallace, R. Lopez, and O. Palacios (1998), Role of plate kinematics and plate-slip-vector partitioning in continental magmatic arcs: Evidence from the Cordillera Blanca, Peru, *Geology*, *26*, 827–830, doi:10.1130/0091-7613(1998)026<0827:ROPKAP>2.3.CO;2.

McQuarrie, N., B. K. Horton, G. Zandt, S. Beck, and P. G. DeCelles (2005), Lithospheric evolution of the Andean fold-thrust belt, Bolivia, and the origin of the central Andean plateau, *Tectonophysics*, *399*, 15–37, doi:10.1016/j.tecto.2004.12.013.

Morand, V. J. (1992), Pluton emplacement in a strike-slip fault zone: The Doctors Flat Pluton, Victoria, Australia, *J. Struct. Geol.*, *14*, 205–213, doi:10.1016/0191-8141(92)90057-4.

Moreau, C., D. Demaiffe, Y. Bellion, and A. M. Boullier (1994), A tectonic model for the location of the Palaeozoic ring complexes in Aïr (Niger, West Africa), *Tectonophysics*, *234*, 129–146, doi:10.1016/0040-1951(94)90208-9.

Müller, J. P., J. Kley, and V. Jacobshagen (2002), Structure and Cenozoic kinematics of the Eastern Cordillera, southern Bolivia (21°S), *Tectonics*, *21*(5), 1037, doi:10.1029/2001TC001340.

Olson, S. F., and N. Gilzean (1987), *Informe Interno de Avance de El Quevar Project*, Minera Utah, Salta, Argentina.

Oncken, O., D. Hindle, J. Kley, K. Elger, P. Victor, and K. Schemmann (2006), Deformation of the Central Andean Upper Plate System—Facts, fiction, and constraints for plateau models, in *The Andes—Active Subduction Orogeny*, edited by O. Oncken et al., pp. 3–27, Springer, Berlin.

Ouimet, W. B., and K. L. Cook (2010), Building the Central Andes through axial lower crustal flow, *Tectonics*, *29*, TC3010, doi:10.1029/2009TC002460.

Petrinovic, I. A. (1999), La caldera de colapso del Cerro Aguas Calientes, Salta, Argentina: Evolución y esquema estructural, in *Geología de los Andes Centrales Meridionales: El Noroeste Argentino*, edited by F. Colombo, I. Queralt, and I. A. Petrinovic, *Acta Geol. Hisp.*, *34*, 243–253.

Petrinovic, I. A., and F. Colombo Piñol (2006), Phreatomagmatic and phreatic eruptions in locally extensive settings of southern Central Andes: The Tocomar volcanic centre (24°10′S–66°34′W), Argentina, *J. Volcanol. Geotherm. Res.*, *158*, 37–50, doi:10.1016/j.jvolgeores.2006.04.013.

Petrinovic, I. A., J. Mitjavila, J. G. Viramonte, J. Marti, R. Becchio, J. M. Arnosio, and F. Colombo (1999), Descripción geoquímica y geochronológica de secuencias volcánicas neógenas de Trasarco, en el extremo oriental de la Cadena Volca' nica Transversal del Quevar (noroeste de Argentina), in *Geológia de los Andes Centrales Meridionales: El Noroeste Argentino*, edited by F. Colombo, I. Queralt, and I. A. Petrinovic, *Acta Geol. Hisp.*, *34*, 255–272.

Petrinovic, I. A., U. Riller, and J. A. Brod (2005), The Negra Muerta volcanic complex, southern Central Andes: Geochemical characteristics and magmatic evolution of an episodically active volcanic centre, *J. Volcanol. Geotherm. Res.*, *140*, 295–320, doi:10.1016/j.jvolgeores.2004.09.002.

Petrinovic, I. A., U. Riller, G. Alvarado, J. A. Brod, and M. Arnosio (2006), Bimodal volcanism in a tectonic transfer zone: Evidence for tectonically controlled magmatism in the southern Central Andes, NW Argentina, *J. Volcanol. Geotherm. Res.*, *152*, 240–252, doi:10.1016/j.jvolgeores.2005.10.008.

Petrinovic, I. A., J. Martí, G. J. Aguirre-Díaz, S. Guzmán, A. Geyer, and N. Salado Paz (2010), The Cerro Águas Calientes caldera, NW Argentina: An example of a tectonically controlled, polygenetic collapse caldera, and its regional significance, *J. Volcanol. Geotherm. Res.*, *194*, 15–26, doi:10.1016/j.jvolgeores.2010.04.012.

Ramelow, J., U. Riller, R. L. Romer, and O. Oncken (2006), Kinematic link between episodic trapdoor collapse of the Negra Muerta Caldera and motion on the Olacapato–El Toro Fault Zone, southern central Argentina, *Int. J. Earth Sci.*, *95*, 529–541, doi:10.1007/s00531-005-0042-x.

Ramos, V. A. (2008), The basement of the Central Andes, *Annu. Rev. Earth Planet. Sci.*, *36*, 289–324, doi:10.1146/annurev.earth.36.031207.124304.

Richards, J., and M. Villeneuve (2002), Characteristics of late Cenozoic volcanism along the Archibarca lineament from Cerro Llullaillaco to Corrida de Cori, northwest Argentina, *J. Volcanol. Geotherm. Res.*, *116*, 161–200, doi:10.1016/S0377-0273(01)00329-8.

Riller, U., and O. Oncken (2003), Growth of the central Andean Plateau by tectonic segmentation is controlled by the gradient in crustal shortening, *J. Geol.*, *111*, 367–384, doi:10.1086/373974.

Riller, U., I. Petrinovic, J. Ramelow, M. Strecker, and O. Onken (2001), Late Cenozoic tectonism, collapse caldera and plateau formation in the Central Andes, *Earth Planet. Sci. Lett.*, *188*, 299–311, doi:10.1016/S0012-821X(01)00333-8.

Risse, A., R. B. Trumbull, B. Coira, S. M. Kay, and P. van den Bogaard (2008), $^{40}Ar/^{39}Ar$ geochronology of mafic volcanism in the back-arc region of the southern Puna plateau, Argentina, *J. South Am. Earth Sci.*, *26*, 1–15, doi:10.1016/j.jsames.2008.03.002.

Salfity, J. A. (1985), Lineamentos transversales al rumbo andino en el noroeste argentino, in *Actas IV Congreso Geológico Chileno*, vol. 2, pp. 119–137, Asoc. Geol. Argentina, Antofagasta, Chile.

Salfity, J. A., and R. A. Marquillas (1994), Tectonic and sedimentary evolution of the Cretaceous-Eocene Salta Group Basin, Argentina, in *Cretaceous Tectonics of the Andes*, edited by J. A. Salfity, pp. 266–315, Vieweg, Brunswick, Germany.

Sato, H. (1994), The relationship between late Cenozoic tectonic events and stress field and basin development in northeast Japan, *J. Geophys. Res.*, *99*, 22,261–22,274, doi:10.1029/94JB00854.

Schreiber, U., and K. Schwab (1991), Geochemistry of Quaternary shoshonitic lavas related to the Calama–Olacapato–El Toro Lineament, NW Argentina, *J. South Am. Earth Sci.*, *4*, 73–85, doi:10.1016/0895-9811(91)90019-H.

Schurr, B., G. Asch, A. Rietbrock, R. Kind, M. Pardo, B. Heit, and T. Monfret (1999), Seismicity and average velocities beneath the Argentine Puna plateau, *Geophys. Res. Lett.*, *26*, 3025–3028, doi:10.1029/1999GL005385.

Schurr, B., G. Asch, A. Rietbrock, R. B. Trumbull, and C. Haberland (2003), Complex patterns of fluid and melt transport in the central Andean subduction zone revealed by attenuation tomography, *Earth Planet. Sci. Lett.*, *215*, 105–119, doi:10.1016/S0012-821X(03)00441-2.

Schurr, B., A. Rietbrock, G. Asch, R. Kind, and O. Oncken (2006), Evidence for lithospheric detachment in the Central Andes from local earthquake tomography, *Tectonophysics*, *415*, 203–223, doi:10.1016/j.tecto.2005.12.007.

Sillitoe, R. H. (1977), Permo-carboniferous, Upper Cretaceous, and Miocene porphyry copper-type mineralization in the Argentinian Andes, *Econ. Geol.*, *72*, 99–103, doi:10.2113/gsecongeo.72.1.99.

Sobel, E. R., G. E. Hilley, and M. R. Strecker (2003), Formation of internally drained contractional basins by aridity-limited bedrock incision, *J. Geophys. Res.*, *108*(B7), 2344, doi:10.1029/2002JB001883.

Spang, J. H. (1972), Numerical method for dynamic analysis of calcite twin lamellae, *Geol. Soc. Am. Bull.*, *83*, 467–471, doi:10.1130/0016-7606(1972)83[467:NMFDAO]2.0.CO;2.

Sperner, B., and P. Zweigel (2010), A plea for more caution in fault-slip analysis, *Tectonophysics*, *482*, 29–41, doi:10.1016/j.tecto.2009.07.019.

Spinks, K., V. Acocella, J. Cole, and K. Bassett (2005), Structural control of volcanism and caldera development in the transtensional Taupo Volcanic Zone, New Zealand, *J. Volcanol. Geotherm. Res.*, *144*, 7–22, doi:10.1016/j.jvolgeores.2004.11.014.

Tibaldi, A. (1992), The role of transcurrent intra-arc tectonics in the configuration of a volcanic arc, *Terra Nova*, *4*, 567–577, doi:10.1111/j.1365-3121.1992.tb00598.x.

Trumbull, R. B., U. Riller, O. Oncken, E. Scheuber, K. Munier, and F. Hongn (2006), The time-space distribution of Cenozoic volcanism in the south-central Andes: A new data compilation and some tectonic implications, in *The Andes—Active Subduction Orogeny*, edited by O. Oncken et al., pp. 29–43, Springer, Berlin.

Turner, F. J. (1953), Nature and dynamic interpretation of deformation lamellae in calcite of three marbles, *Am. J. Sci.*, *251*, 276–298, doi:10.2475/ajs.251.4.276.

Turner, J. C. M. (1964), Descripción geológica de la Hoja 7c, Nevados de Cachi, prov. Salta, *Bol. 99*, Dir. Peral de Geol. y Miner., Buenos Aires.

Twiss, R. J., and J. R. Unruh (1998), Analysis of fault-slip inversion: Do they constrain stress or strain rate?, *J. Geophys. Res.*, *103*, 12,205–12,222, doi:10.1029/98JB00612.

Vezzoli, L., M. Matteini, N. Hauser, R. Omarini, R. Mazzuoli, and V. Acocella (2009), Non-explosive magma-water interaction in a continental setting: Miocene examples from the Eastern Cordillera (Central Andes; NW Argentina), *Bull. Volcanol.*, *71*, 509–532, doi:10.1007/s00445-008-0239-5.

Vigneresse, J. L. (1995), Control of granite emplacement by regional deformation, *Tectonophysics*, *249*, 173–186, doi:10.1016/0040-1951(95)00004-7.

Viramonte, J. G., and I. A. Petrinovic (1990), Cryptic and partially buried calderas along a strike-slip fault system in the Central Andes, *ISAG Grenoble*, edited by Inst. Français de Rech. Sci., pp. 317–320, Ed. de l'Orstom, Paris.

Viramonte, J. G., R. H. Omarini, V. Araña Saavedra, A. Aparicio, and L. Garcia Cacho (1984), Edad génesis y mecanismos de erupción de las riolítas granatíferas de San Antonio de Los Cobres, provincia de Salta, in *IX Congreso Geológico Argentino*, vol. 3, pp. 216–233, Asoc. Geol. Argentina, Bariloche, Argentina.

Wagner, R., C. L. Rosenberg, M. R. Handy, C. Möbus, and M. Albertz (2006), Fracture-driven intrusion and upwelling of a mid-crustal pluton fed from a transpressive shear zone—The Rieserferner pluton (Eastern Alps), *Geol. Soc. Am. Bull.*, *118*, 219–237, doi:10.1130/B25842.1.

White, S. M., J. A. Crisp, and F. J. Spera (2006), Long-term volumetric eruption rates and magma budgets, *Geochem. Geophys. Geosyst.*, *7*, Q03010, doi:10.1029/2005GC001002.

Wilson, C. J. N. (1996), Taupo's atypical arc, *Nature*, *379*, 27–28, doi:10.1038/379027a0.

Yuan, X., S. V. Savolev, and R. Kind (2002), New data on Moho topography in the Central Andes and their geodynamic implications, *Earth Planet. Sci. Lett.*, *199*, 389–402, doi:10.1016/S0012-821X(02)00589-7.

V. Acocella, Dipartimento Scienze Geologiche, Università Roma Tre, Largo San Leonardo Murialdo, 1, I-00146 Roma, Italy. (acocella@uniroma3.it)

A. Gioncada and R. Mazzuoli, Dipartimento di Scienze della Terra, Università di Pisa, I-56126 Pisa, Italy.

R. Omarini, Facultad de Ciencias Naturales, Universidad Nacional de Salta, CONICET, Salta, CP 4400, Argentina.

U. Riller, School of Geography and Earth Sciences, McMaster University, 1280 Main St. W., Hamilton, ON L8S 4K1, Canada.

L. Vezzoli, Dipartimento Scienze Chimiche e Ambientali, Università dell'Insubria, I-22100 Como, Italy.